Analysis of Heat Transfer in Air Cooled Condensers

Sigríður Bára Ingadóttir

Faculty of Industrial Engineering, Mechanical Engineering and Computer Science
University of Iceland
2014

ANALYSIS OF HEAT TRANSFER IN AIR COOLED CONDENSERS

Sigríður Bára Ingadóttir

30 ECTS thesis submitted in partial fulfillment of a
Magister Scientiarum degree in Mechanical Engineering

Advisors
Halldór Pálsson, Associate Professor, University of Iceland
Óttar Kjartansson, Green Energy Group AS
Gestur Bárðarson, Green Energy Group AS

Faculty Representative
Ármann Gylfason, Associate Professor, Reykjavík University

Faculty of Industrial Engineering, Mechanical Engineering and Computer Science
School of Engineering and Natural Sciences
University of Iceland
Reykjavik, May 2014

Analysis of Heat Transfer in Air Cooled Condensers
Analysis of Heat Transfer in ACCs
30 ECTS thesis submitted in partial fulfillment of a M.Sc. degree in Mechanical Engineering

Faculty of Industrial Engineering, Mechanical Engineering and Computer Science
School of Engineering and Natural Sciences
University of Iceland
VRII, Hjardarhagi 2-6
107, Reykjavik, Reykjavik
Iceland

Telephone: 525 4000

Bibliographic information:
Sigríður Bára Ingadóttir, 2014, Analysis of Heat Transfer in Air Cooled Condensers, M.Sc. thesis, Faculty of Industrial Engineering, Mechanical Engineering and Computer Science, University of Iceland.

Printing: Háskólaprent, Fálkagata 2, 107 Reykjavík
Reykjavik, Iceland, May 2014

Abstract

Condensing units at geothermal power plants containing surface condensers and cooling towers utilize great amounts of water. Air cooled condensers (ACCs) are not typically paired with dry or flash steam geothermal power plants, but can be a viable solution to eliminate the extensive water usage and vapor emissions related to water cooled systems. The present thesis investigates two different models that provide tools for calculating the heat transfer coefficient across air cooled tube bundles. An analytical model is created using MATLAB (2013), while ANSYS Fluent (2013a) is used to generate a numerical model. A correlation from literature is used for the heat transfer coefficient calculation in the analytical model and the $k-\omega$ shear stress transport (SST) turbulence model is used in ANSYS Fluent (2013a). When compared, the analytical model results in more accuracy than the numerical model. However, both models can be utilized to optimize air cooled condenser design.

Útdráttur

Kælikerfi í jarðvarmaverum sem notast við varmaskipta ásamt kæliturnum kalla á töluverða vatnsnotkun. Loftkældir eimsvalar eru raunhæf lausn til þess að koma í veg fyrir óþarfa sjónmengun og mikla vatnsnotkun. Vanalega eru loftkældir eimsvalar ekki nýttir við jarðvarmaver og er því brýnt að skoða þá lausn. Í ritgerðinni eru tvö líkön sett fram þar sem hvort þeirra býður upp á möguleika á útreikningum á varmaleiðnistuðli yfir loftkæld rör með kæliplötum. Greiningin er framkvæmd fræðilega í forritinu MATLAB (2013) en einnig er notast við tölulega greiningu í ANSYS Fluent (2013a). Þá er notast við jöfnur úr fræðigreinum til að framkvæma útreikninga fræðilega en tölulega er notast við $k-\omega$ SST iðustreymislíkanið í ANSYS Fluent (2013a). Þegar líkönin eru borin saman er greinilegt að fræðilega nálgunin er nákvæmari, en tölulega nálgunin býður upp á sjónræna túlkun af flæðinu. Hinsvegar geta bæði líkönin verið notuð í bestun á loftkældum eimsvölum.

Contents

List of Figures

List of Tables

Nomenclature

Abbreviations

ACC	Air Cooled Condenser
GEA	GEA Power Cooling Inc.
GEG	Green Energy Group AS
$PISO$	Pressure-Implicit with Splitting of Operators
SST	Shear Stress Transport

Constants

g	Acceleration due to gravity	[m/s^2]

Greek Letters

ϵ_{rel}	Relative error	[%]
η_c	Cold side fin efficiency	
η_h	Hot side fin efficiency	
μ	Viscosity	[kg/ms]
ρ	Density	[kg/m^3]

Subscripts

a	Air with properties evaluated at inlet
l	Liquid phase
L	Large
n	Row number
S	Small
s	Steam with properties evaluated at inlet

v	Vapor phase	

Variables

A_c	Total cross-sectional area of all steam inlets	[m^2]
A_c	Cold side, single tube area	[m^2]
A_f	Total face area of bundle row 1	[m^2]
A_h	Hot side, single tube area	[m^2]
C_d	Coefficient of drag	
C_l	Coefficient of lift	
C_p	Constant pressure specific heat	[J/kg K]
D_f	Fin diameter	[m]
D_i	Tube inner diameter	[m]
D_o	Tube outside diameter	[m]
G	Mass velocity per area	[kg/m^2s]
h	Heat transfer coefficient	[W/mK]
H_f	Height of fin	[m]
h_{TP}	Two-phase heat transfer coefficient	[W/mK]
i_{fg}	Enthalpy of vaporization at condenser tube inlet	[kJ/kg]
i'_{fg}	Corrected enthalpy of vaporization at condenser tube inlet	[kJ/kg]
i_{in}	Enthalpy of steam at condenser tube inlet	[kJ/kg]
i_{out}	Enthalpy of saturated liquid at condenser tube outlet	[kJ/kg]
k_a	Thermal conductivity of air	[W/m^2K]
k_{st}	Thermal conductivity of steel	[W/m^2K]
L	Tube length	[m]
$\dot{m}$	Mass flow rate	[kg/s]
N_b	Total number of bundles in the condenser	
N_f	Total number of fins per meter	

N_t	Total number of tubes in the condenser	
N_{tn}	Total number of tubes in row n of each bundle	
Nu	Nusselt number	
q	Condenser cooling requirement	[kW]
q_c	Condenser cooling capacity	[kW]
q_{net}	Total heat transfer from tube and fin walls	[kW]
Re	Reynolds number	
s	Average distance between individual fins	[m]
Sr	Strouhal number	
t_m	Fin average thickness	[m]
t_b	Thickness of fin at base	[m]
T_{ci}	Temperature of cold fluid at inlet	[°C]
T_{co}	Temperature of cold fluid at outlet	[°C]
T_g	Saturation temperature of liquid film	[°C]
T_{hi}	Temperature of hot fluid at inlet	[°C]
T_{ho}	Temperature of hot fluid at outlet	[°C]
ΔT_{lm}	Log mean temperature difference	[°C]
t_t	Thickness of fin at fin tip	[m]
T_w	Temperature of the tube wall	[°C]
$\dot{V}$	Volumetric flow rate	[m^3/s]

Acknowledgments

This thesis was done under the supervision of Halldór Pálsson, Associate Professor in the Faculty of Industrial Engineering, Mechanical Engineering and Computer Science in the School of Engineering and Natural Sciences at the University of Iceland. His constant advice, guidance and support kept me afloat throughout my studies. I sincerely thank him for his time, patience, and endless encouragement.

I would like to give thanks to Green Energy Group AS for their financial support throughout the project. Also to Gestur R. Bárðarson and Óttar Kjartansson, without whom this project would never have existed. Thank you for trusting me with this project.

Additionally, I would like to thank Dr. Francine Battaglia, Professor in the Faculty of Mechanical Engineering at Virginia Tech. Thank you for your friendship and incredible support throughout my years at Virginia Tech. Your contagious love for the thermal and fluid sciences led me here. Thank you.

Lastly, thanks to my incredible family and friends. Without you, this ride would have been endless. Thanks mom and dad for your undying support, and for telling me I can do whatever I put my mind to. No matter how many battles were lost - I would win the war.

1. Introduction

A geothermal power plant is quickly recognized from afar due to the visible plume it emits. The plume is a water vapor that is being released into the atmosphere and can be disturbing to the visual experience of a beautiful landscape. The plume is traced to a cooling tower that has been coupled with a condenser unit. Both dry and flash steam geothermal power plants use water cooling exclusively to condense the geothermal steam from turbine exhaust. Water used for cooling purposes is typically extracted from a nearby source such as lakes or rivers (Zammit, 2005). Therefore, water usage becomes an environmental concern when too much is extracted or when water is not readily available. This water cooling system is convenient where water is available and no regulations are in place for water usage (Kagel et al., 2007).

Geothermal fluids consist of different chemical compositions depending on their location but the main chemicals include hydrogen sulfide (H_2S), arsenic (As), boron (B), and mercury (Hg). When discharged into the atmosphere these chemicals can be damaging to the nearby environment. Many regions have stringent regulations about the treatment of the geothermal fluid, therefore requiring full re-injection of the fluid once all energy has been extracted (Kristmannsdóttir and Ármannsson, 2003). Assuming that full re-injection takes place, availability of water for cooling and the resulting visible plume are subjects of concern.

The available water source plays an important role in a water cooled system as the water requirement is continuous for once-through wet cooling systems and for those coupled with a cooling tower. Water cooled systems typically require about 20 liters of cooling water per megawatt hour (Kagel et al., 2007). Therefore, in arid regions where water is scarce, air cooled systems can be a viable alternative. Currently air cooled systems are coupled with binary geothermal power plants (Kagel et al., 2007) and other binary fossil fuel plants. Thus, a modular wellhead solution company by the name of Green Energy Group AS (GEG) poses the question of using an air cooled condenser (ACC) with a flash steam geothermal system. The company contacted an ACC solution vendor by the name of GEA Power Cooling Inc. (GEA) for a budgetary quotation and a preliminary design (Yazbek, 2013). Their design data is used in the present thesis to allow for an applicable solution.

The objective of the thesis is to take a look at the implementation of an ACC unit in a dry or flash steam geothermal power plant. The thesis is organized as follows: First, an extensive literature review is performed on heat transfer and condensation calculation methods. Next, various condensing systems used in geothermal power plants are described and compared to an air cooled condensing unit. Then,

the case being considered is further described and analyzed using an analytical and a numerical model. The methods used for the two models are also discussed in detail. The two models are created to provide separate tools for calculating the cooling capacity of an ACC with staggered tube rows in a tube bundle. As stated earlier, the data for the calculations is provided by a preliminary research performed by GEG (Yazbek, 2013).

The two models use separate methods for calculating the heat transfer coefficient across the tube bundle; a correlation from literature and a numerical model calculation using ANSYS Fluent (2013a). A 2D model of a cylinder in crossflow is created to validate the ANSYS Fluent (2013a) numerical model. Next, a mesh convergence study is performed to prove sufficient mesh refinement for the model calculations. Then, once the two heat transfer coefficients have been calculated, the two models are compared. This thesis thus presents two tools for modeling the heat transfer across a staggered tube bundle in an air cooled condenser unit.

2. Background

2.1. Condensing Systems

Dry and flash steam geothermal power plants require geothermal steam to be condensed after it has traveled through turbines. The process of condensing is most often considered wet or dry depending on the cooling fluid (Zammit, 2005). Condensing systems are also paired with noncondensable gas removal systems. However, for the sake of simplification, these systems are not accounted for in this study. This chapter describes the most common condensing systems in today's power plants, considering both water cooled and air cooled systems.

2.1.1. Water Cooling

Water cooled systems utilize a water source to condense steam from the turbine. These systems require a vast amount of water and geothermal power plants typically use up to 20 liters of freshwater per megawatthour Kagel et al. (2007). This section discusses the two main types of water cooling; once-through and recirculating.

Once-Through Cooling

Conventional shell and tube, or plate-frame surface condensers are utilized in once-through cooling systems. This indirect cooling system utilizes water from a source such as the ocean, rivers or lakes nearby. The water is passed through the surface condenser tubes in order to condense the steam from the turbine (Zammit, 2005). This cooling system is one of the most efficient while most often requiring the lowest capital investment (Mortensen, 2011). A schematic of this process can be seen in figure 2.1.

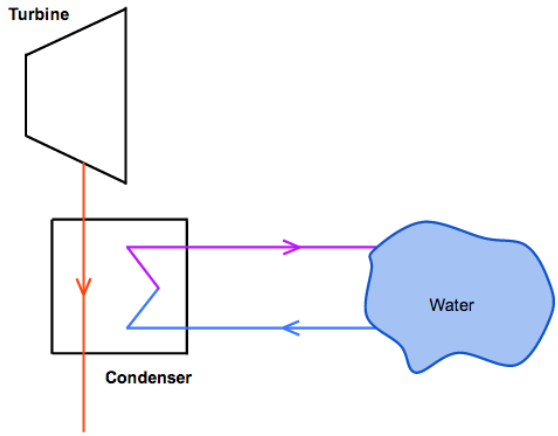

Figure 2.1: Water once-through cooling in a surface condenser

Recirculating Cooling

Like once-through cooling, recirculating cooling systems utilize a surface condenser in order to condense the steam. However, this system utilizes the same waterflow again by cooling it down in a wet cooling tower. The cooling water is then recirculated back into the condenser. The cooling tower causes about 1-2% of the cooling water to evaporate, thus requiring makeup water from nearby water sources (Zammit, 2005). The evaporated cooling water exits the cooling tower as water vapor, causing a visible plume (Kagel et al., 2007).

Recirculating wet cooling requires less water withdrawal than the once-through system. However, a system for the make-up water needs to be implemented to maintain the cooling capacity of the cooling tower. As this system requires both a surface condenser and a cooling tower, it results in a higher capital cost than the once-through cooling system (Mortensen, 2011). A schematic of this system can be seen in figure 2.2.

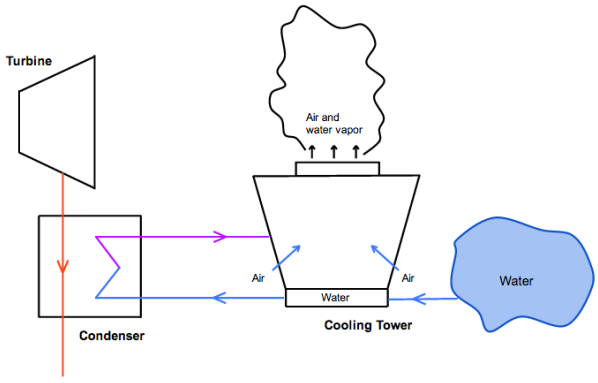

Figure 2.2: Indirect water recirculating cooling system

Recirculating cooling can also be paired with a direct contact condenser, where steam and cooling water are mixed in order to condense the steam. This system also requires water from a local source in order to perform condensation. Plumes are visible from the direct cooling system. A schematic of the system can be seen in figure 2.3.

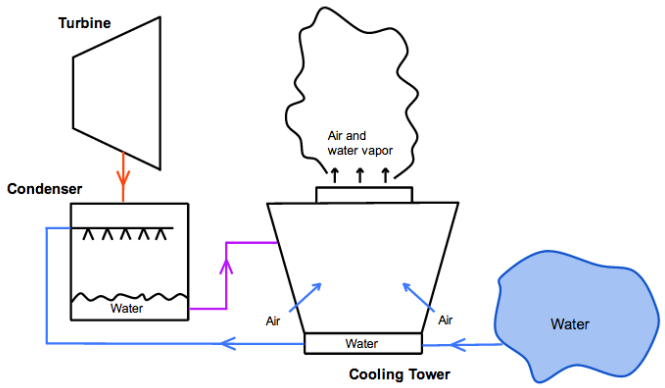

Figure 2.3: Water recirculating cooling in a direct contact condenser

2.1.2. Air Cooling

Air cooled systems rely on convective heat transfer by using the atmospheric air to cool steam in a finned-tube bundle (Conradie and Kröger, 1996). A fan is used to create forced convection. This system is referred to as a direct dry cooling system, as the steam inside the tubes is cooled directly by the ambient air passing over the finned surface. (Mortensen, 2011). The process is shown in figure 2.4.

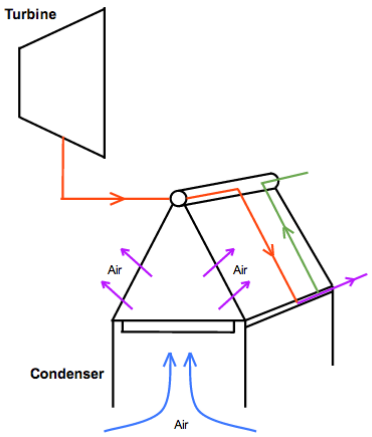

Figure 2.4: A schematic of a dry air cooling system

For a better view of the air cooled condenser, a zoomed view of the tube bundles is shown in figure 2.5

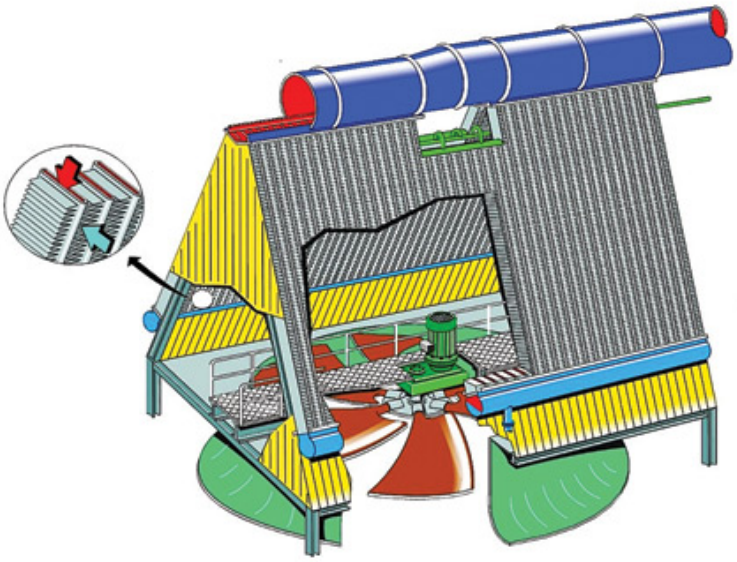

Figure 2.5: A zoomed view of an ACC unit showing the tube bundles (SPX Cooling Technologies Inc.)

Most ACCs have a row in each cell assigned as the *dephlegmator* row, some ACCs contain a cell that is the dephlegmator cell. This row is designed to remove the non-condensable gases from the steam. The uncondensed steam and the entrained non-condensables gather at the bottom of the tube bundles and are carried up through the dephlegmator row, shown as green in figure 2.4. Steam ejectors or compressors are then used to remove the non-condensables from the top of the ACC tube bundle. If steam travels up this row it gets condensed and flows back down (counter-current to entering steam) to the condensate header and finally into the condensate tank (Zammit, 2005).

An air cooled system requires no water for operation and emits no vapor plume. This system is the least efficient of the three, while requiring the highest capital cost (Mortensen, 2011).

2.1.3. Cooling System Summary

When looking at the three types of cooling systems previously described, it is interesting to see how they compare. Table 2.1 lists the main elements for comparison and if the element is present in the corresponding system it is marked by “x”.

Table 2.1: Comparison between condensing systems

System	Water Required	Visible Plume	Capital Cost	Efficiency
Once-Through Cooling	x		Low	High
Recirculating Cooling	x	x	Medium	High
Air Cooling			High	Low

From the table it is evident that air cooling is not ideal for power plants on a low budget. Due to the high capital cost it is of utmost importance to design these units for an effective performance. As mentioned before, an air cooled condenser does not rely on any water sources nearby for cooling purposes (Conradie and Kröger, 1996). Thus, air cooled systems can prove useful in those areas where environmental regulations are stringent and water is scarce.

2.2. Heat Exchangers

An extensive literature review is performed to introduce the current state of heat transfer research. The literature review is separated into the two sections; finned tube heat transfer and condensation in inclined tubes.

2.2.1. Finned Tube Heat Transfer

Heat transfer coefficients across individually finned tube bundles in crossflow were studied in detail by Briggs and Young (1963). Their experiment was aimed at providing a good correlation for the heat transfer coefficient as a function of the number of tube rows. Data was also gathered in order to determine how the air film heat transfer coefficient is affected by fin thickness and tube pitch. Their correlation for the Nusselt number across a tube bundle works for any number of tube rows, taking into account fin height, thickness, spacing and root diameter to give accurate results.

The crossflow case was also studied by Gray and Webb (1986). They used multiple regression techniques to develop a correlation for the Nusselt number over a plate-finned tube bundle. Their correlation can only be applied to tube bundles with four or more rows. However, Gray and Webb also developed a multiplication

factor for the row effect, if the number of rows is less than four. According to their research, the correlation developed by Briggs and Young (1963) can be applied to plate-finned tubes as well if the fin tips are assumed to be touching.

A crossflow heat transfer coefficient correlation for finned-tube bundles has also been studied for various fin types. Hofmann et al. (2007) studied the I-shaped and U-shaped fin geometries on serrated and solid fins. The main purpose of their study was to investigate the difference between heat transfer and pressure drop in serrated and solid fins as well as the effect of various geometries. They concluded that increased fin height leads to a lower heat transfer coefficient while no substantial differences were recorded for the two types of fins.

2.2.2. Condensation in Inclined Tubes

Condensation in inclined tubes has been studied since the 1960s when Chato (1960) performed his doctoral research on condensation in horizontal and inclined tubes. His research showed that increasing the inclination of downward flow in slightly inclined tubes led to a higher heat transfer coefficient. Chato's study is frequently referenced and his correlation is the leading correlation in condensation calculations. Shah (1979) studied the whole range of inclination angles in order to develop a dimensionless correlation for predicting a two-phase heat transfer coefficient. The correlation was developed from 21 independent studies using various fluids (water, R-22, ethanol, etc.) at horizontal, vertical, and inclined orientations with diameters ranging from 7 mm to 40 mm. This heat transfer coefficient showed good agreements for film condensation inside pipes at any inclination. Kim and No (1999) studied Shah's correlation even further, using it to develop their own correlation for the two-phase heat transfer coefficient for condensation in a larger diameter vertical tube. They utilized wall temperatures to develop the correlation for turbulent annular film condensation. For these conditions, Kim and No's model correlates better than Shah's model.

More recently, condensation in inclined tubes was studied by Würfel et al. (2003). Their study mainly considered the condensation of organic vapors. A correlation for the Nusselt number of the flow was developed in terms of the inclination angle. The film thickness and friction coefficient were studied as well as their relationship to the shear controlled flow. According to their study, the friction coefficient should not be neglected during experiments on two-phase flow. Today, research is still being performed on condensation in inclined tubes as the phenomena is still a topic of interest. Lips and Meyer (2011c) performed an extensive literature review on condensation in inclined tubes and concluded that there is a lack of experimental studies for the subject. In their review, they not only highlighted the importance of understanding the relationship between inclination angles and flow patterns, but also the angle's relationship to the pressure drop and heat transfer coefficient of the two phase flow.

Lips an Meyer claimed that more experimental studies were needed to develop a better understanding of this flow, thus they performed their own study of convective condensation in an inclined smooth tube, using R134a as their working fluid. Their study focused on two parts; the inclination angle's relationship to the flow pattern and heat transfer coefficient (Lips and Meyer, 2011a), and the angle's relationship to void fractions and pressure drops (Lips and Meyer, 2011b). From the first part of their study they concluded that the flow pattern is strongly dependent on the inclination angle for low mass fluxes and/or low vapor qualities. On the other hand, high mass fluxes and high vapor qualities resulted in constant annular flow regardless of the inclination angle. The second part of their study focused on comparing their experimental results to correlations from available literature. The pressure drop in vertical upward flow showed good agreement with the correlations available, whereas no correlations from literature predicted the downward flow correctly. Similar results were found for the void fraction relationship. Later, the pair created a stratified flow model for convective condensation in an inclined tube (Lips and Meyer, 2012). They focused the experiment on finding the optimum inclination angle leading to the highest heat transfer coefficient for stratified flow. Their experiment concluded that the curvature of the liquid-vapor interface is significant in predicting the heat transfer coefficient. They also found that the optimum inclination angle for downward flow is 45° when taking into account the liquid-vapor curvature.

Meyer was joined by Dirker and Adelaja to investigate condensation at different saturation temperatures (Meyer et al., 2013). This study also used R134a as the working fluid in smooth inclined tubes and showed that the heat transfer coefficient decreased with increasing saturation temperature at all inclination angles. The inclination angle range of -90° to 90° was also studied by Akhavan-Behabadi et al. (2007) when they studied condensation inside a microfin tube at the various inclination angles. They developed a correlation for the heat transfer coefficient inside a microfinned tube and concluded that the inclination strongly affected the heat transfer coefficient. According to their study, the inclination angle highly affects flows of low vapor qualities and low mass velocities.

Laminar film condensation was studied in tubes with a diameter less than 5 mm by Wang and Du (1999). Their study aimed to explore the effects of various forces on the process of condensation. A model was created to evaluate the significance of these forces and they concluded that the flow regime is not shaped by gravity forces in small/mini diameter tubes. A similar study was performed by Wang et al. (1998) where a small/mini diameter tubes were utilized to perform visual experiments on flow patterns of various R-11 vapor qualities at different inclination angles. They concluded that the gravitational force significantly impacts flow patterns in condensation in-tube. Additionally, they developed correlations that predict the flow pattern transition location.

Elliptical Tubes

Chiou et al. (1994) expected elliptical tubes to provide higher heat transfer coefficients than circular ones due to the different surface tension. However, their study proved that surface tension effects only impacted the tube's hydrodynamic characteristics and the local heat transfer coefficient. The effect on the mean heat transfer coefficient were close to insignificant.

Despite the findings of Chiou et al. (1994), Hu and Chen (2005) studied turbulent film condensation in inclined elliptical tubes. The main aspects of their research were the heat transfer coefficient and local condensate film thickness in the elliptical tubes. Their study concluded that circular tubes are recommended for a forced convective condensation, whereas elliptical tubes are recommended for natural convective condensation. Therefore, this thesis will only consider convective condensation in circular tubes.

Noncondensable gases

Factors such as concentration of noncondensable gases cause a reduction in heat transfer in condensation systems. Caruso et al. (2013) studied the effect of noncondensable gases on the local heat transfer coefficient during the condensation of steam in inclined tubes. Their study was performed on a wide range of noncondensable gas concentration in order to evaluate the optimum system configuration. Caruso et al. concluded that with increasing Reynolds numbers of the liquid-vapor-noncondensable gas mixture, the local heat transfer coefficient increases. The correlation of the mixed steam-air condensation heat transfer coefficient appeared to be in good agreement with their experimental results. Caruso and Vitale Di Maio (2013) then applied a heat and mass transfer analogy to the condensation with the presence of noncondensable gases in inclined tubes. They developed a correlation based mainly on dimensionless numbers and compared it to previously developed models. An agreement was found when their model was verified against the model created by Chato (1960). It was clear that Chato's (1960) model still proved the best for condensation inside tubes.

3. Materials and Methods

This chapter discusses the materials obtained for this study. It also describes the analytical model in detail where the correlation developed by Chato (1960) is used for internal flow calculations and the correlation developed by Briggs and Young (1963) is used for external flow. The numerical model is then described where the Navier-Stokes equations are discussed along with the energy equation. These equations represent the fundamental calculations for the simulation, but the k-ω shear stress stransport (SST) model is chosen to represent the turbulence.

3.1. ACC Materials

Green Energy Group AS (GEG) currently operates three modular wellhead plants in Kenya (Green Energy Group, 2014). Due to the arid regions in Africa, GEG is considering having the option of implementing an air cooled condenser in their system if required by their customer. Therefore, data has been gathered on available complete air cooled condenser systems. A preliminary design was made by an air cooled condenser manufacturer by the name of GEA Power Cooling Inc. The solution is specifically designed for a modular wellhead power plant currently in operation. The original information provided for the air cooled condenser design is found in table 3.1.

Table 3.1: Main specifications for the air cooled condenser design

Variable	**Value**
Turbine Back Pressure [bar-a]	0.1
Design Ambient Temp. [°C]	20
Design Steam Flow [kg/s]	7
Steam Enthalphy [kJ/kg]	2300
Dryness Factor [%]	87
Site Elevation [mamsl]	2010

GEA used the information from table 3.1 to design an air cooled condenser suitable for the 3.2 MW power production required by GEG. The materials are chosen for minimum corrosion in the corrosive geothermal environment. Therefore, stainless steel 316L is chosen for the tubes which is paired with Aluminum Alloy 1060 for the fins. The air cooled condenser design is comprised of one street with two bays where each bay has one fan. This configuration is shown in figure 3.1, where the bays are numbered as one and two.

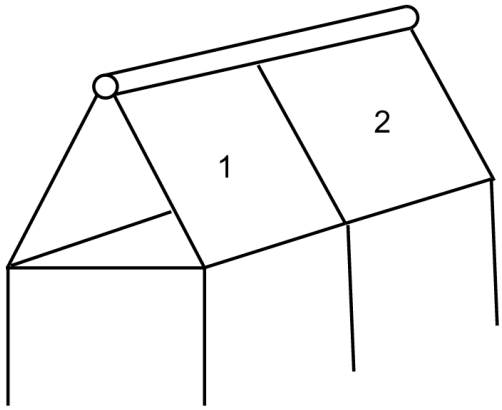

Figure 3.1: A typical A-frame ACC street with two bays

Larger systems can have multiple streets which are lined up next to each other. Table 3.2 shows the main information for the GEA design.

Table 3.2: ACC Unit Solution from GEA

Variable	**Value**
Number of Streets	1
Number of Bays	2
Number of Tube Rows/ Bundle	4
Total Number of Tube Bundles	12
Total Number of Finned Tubes/Bundle	146
Total Number of Fans	2
Tube Diameter [mm]	50.80 / 38.1
Number of fins per meter	354 / 394
Tube Thickness [mm]	1.65
LMTD [°C]	15.50
U, Finned Tube [W/m^2·°C]	21.52
U, Clean Bare Tube [W/m^2·°C]	390.77

This study uses the design provided by GEA to create analytical and numerical models. As seen in the table the total number of tube rows per bundle is four, with

146 tubes per bundle. Therefore, the total number of tubes in the street is 1752. These finned tubes contain annular fins with a trapezoidal cross section, as seen in figure 3.2, where t_b is the thickness at the base, and t_t is thickness at the tip.

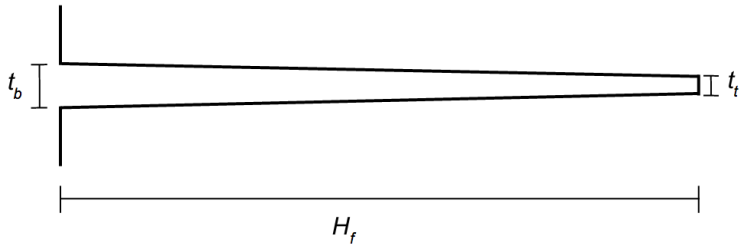

Figure 3.2: The fins are designed to have a trapezoidal cross section

The fin strip is wound into a mechanically produced groove on the tube and tightened by backfilling of the base material under pressure. The groove is 0.3 mm deep and provides high fin stability, increased heat transfer and allows for a high operating temperature (Yazbek, 2013). For simplification it is assumed that the fin base has full contact with the tube without being located in a groove, as displayed in figure 3.3. It is also assumed that the fin thickness is the average thickness of the trapezoidal fin. Therefore, the average fin thickness is represented as t_m.

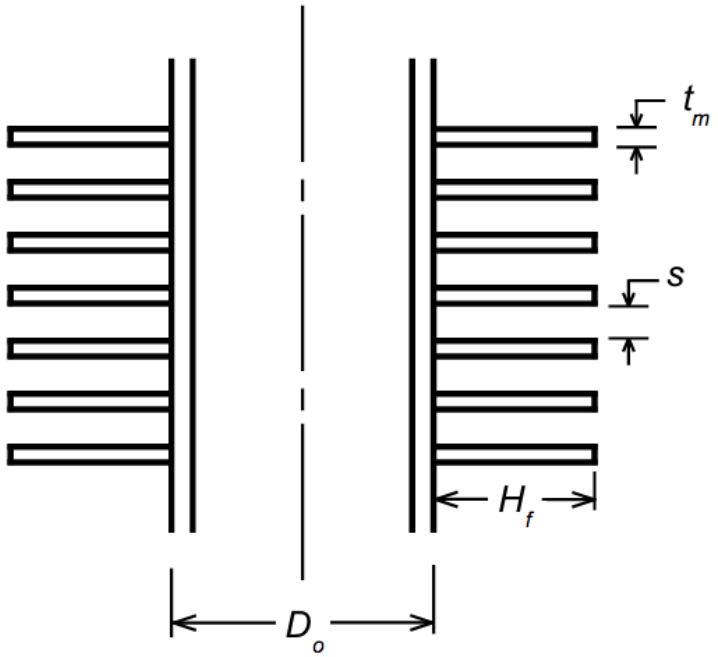

Figure 3.3: The cross section of the tube bundle shows averaged fin thickness

The finned tubes are located in four separate rows, with varying diameters. Rows one and two both have large diameters; 50.8 mm tube diameter and 82.55 mm fin

diameter. On the other hand, rows three and four have the smaller diameters; 38.1 mm tube diameter and 68.95 mm fin diameter. Due to the size difference in the tubes, the number of fins per meter also varies. The total number of fins on the large tube is 354 when on the small tubes it is 394. For simplification, the fin spacing is assumed to be the average of the two sizes, making the spacing the same for all tubes.

The tubes are staggered with a triangular pitch of 95 mm. A portion of the tube bundle is shown in figure 3.4, where the rows are numbered on top.

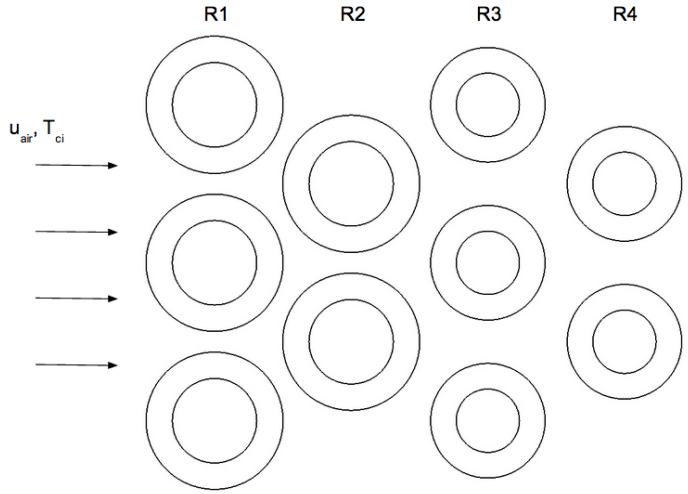

Figure 3.4: The finned tube bundle is designed to have four rows of tubes

Row 4 is the dephlegmator row, where non-condensable gases flow up. Therefore, steam leaving the turbine does not enter row 4 at the top. The schematic of the condenser and the data sheet obtained from GEA (Yazbek, 2013) can be referred to in Appendix A for further information.

3.2. Analytical Model

An analytical model of the tube bundle in the ACC is created using MATLAB (2013) to acquire results close to the data sheet provided by GEA. Heat transfer through the air cooled condenser system is calculated by analyzing the two flows; internal and external. The internal flow represents the two phase flow that flows inside the condenser tubes. The external flow, however, is the air flowing in crossflow through the tube bundle with staggered tubes. Correlations from literature are utilized to solve for the respective heat transfer coefficients.

First, the total cooling requirement is calculated. The cooling requirement is

written as an energy balance for the condenser,

$$q = \dot{m}_s(i_{in} - i_{out}) \tag{3.1}$$

where $\dot{m}_s$ is the total mass flow rate from the turbine and i denotes the corresponding enthalpies. Then, the log mean temperature difference for the system is found using the following equation

$$\Delta T_{lm} = \frac{\Delta T_2 - \Delta T_1}{\ln\left(\frac{\Delta T_2}{\Delta T_1}\right)} \tag{3.2}$$

where ΔT_2 and ΔT_1 are defined as

$$\Delta T_2 = T_{hi} - T_{ci}$$

$$\Delta T_1 = T_{ho} - T_{co}$$

with T_h representing the hot fluid inside the tube at either inlet or outlet, and T_c representing cold air at inlet or outlet.

Then the overall condenser capacity can be solved for using the following equation

$$q_c = UA\Delta T_{lm} \tag{3.3}$$

The overall heat transfer coefficient, U, is then essential in calculating the actual cooling capacity of the designed ACC. The calculation is dependent on the internal and external heat transfer coefficients.

3.2.1. Internal Flow

The main component of the internal flow is the two-phase heat transfer coefficient. In order to calculate the two-phase heat transfer the correlation developed by Chato (1960) is used. First, the total cross-sectional area is calculated for all tube inlets where steam enters.

$$A_c = \frac{\pi}{2}\left[D_{iL}^2\frac{N_t}{4} + D_{iS}^2\frac{N_t}{2}\right] \tag{3.4}$$

where D_{iL} and D_{iS} are the large and small inner diameters respectively, and N_t is the total number of tubes in the system. Next, the mass flow rate per area is calculated for each tube

$$G_s = \frac{\dot{m}_s}{A_c} \tag{3.5}$$

where $\dot{m}_s$ is the total mass flow rate of steam leaving the turbine exhaust. Then, the respective Reynolds numbers can be calculated for the vapor and liquid using the following equation

$$Re = \frac{D_i G_s}{\mu} \tag{3.6}$$

where D_i is the inner diameter of the tube and μ is the dynamic viscosity of either liquid or vapor. Next, the two-phase heat transfer coefficient is calculated using the equation developed by Chato (1960) for laminar flow inside horizontal tubes altered for inclined tubes.

$$h_{TP} = 0.555 \left[\frac{\rho_l(\rho_l - \rho_v) g' k_l^3 i'_{fg}}{\mu_l D_i (T_g - T_w)} \right]^{1/4} \tag{3.7}$$

where T_g is the saturation temperature of the liquid film, T_w is the tube wall temperature, k_l is the thermal conductivity of the liquid, and g' is defined by the following equation

$$g' = g \sin(\theta) \tag{3.8}$$

where g is the gravitational acceleration constant and θ is the angle of inclination. The corrected enthalpy of vaporization is defined as

$$i'_{fg} = i_{fg} + 0.357 C_{pl}(T_g - T_w) \tag{3.9}$$

where the tube wall temperature (T_w) is assumed to be close to the saturation temperature of the liquid.

3.2.2. External Flow

External flow calculations are performed using the correlation developed by Briggs and Young (1963) for an average heat transfer coefficient across an annular finned tube bundle. First, the total face area is calculated in order to calculate the air face velocity. The total face area is defined as

$$A_f = N_{t1} N_b \left[D_f (L - L N_f t_b) + 2(N_f - 1) H_f \left(\frac{t_b}{2} - \frac{t_t}{2} \right) \right] \tag{3.10}$$

where N_{t1} is the number of tubes in row one, N_b is the total number of bundles in the system, D_f is the diameter of the fin, L is the length of the tube, and N_f is the total number of fins per meter. The fin height, H_f, is found with the following equation

$$H_f = \frac{1}{2} (D_f - D_o) \tag{3.11}$$

where D_o is the outside diameter. Next, the mass flow rate of the air is calculated:

$$\dot{m}_a = \frac{\dot{V}_a}{\rho_a} \tag{3.12}$$

where $\dot{V}_a$ is the volumetric flow rate of air through the fan, and ρ_a is the density of air. Finally, the Reynolds number for the air is calculated in the following way

$$Re_a = \frac{D_o G_a}{\mu_a} \tag{3.13}$$

where G is defined as

$$G_a = \frac{\dot{m}_a}{A_f} \tag{3.14}$$

Therefore, the inlet face velocity is defined as

$$u_a = \frac{G_a}{\rho_a} \tag{3.15}$$

The correlation developed by Briggs and Young (1963) allows for a calculation of the Nusselt number across a staggered tube bundle. The correlation is as follows

$$Nu_a = 0.134 Re_a^{-0.319} \left[\frac{s}{H_f}\right]^{0.2} \left[\frac{s}{t_m}\right]^{0.11} \tag{3.16}$$

where t_m is defined as

$$t_m = \frac{t_b + t_t}{2} \tag{3.17}$$

and s is the average spacing between two fins

$$s = \frac{1}{2}\left[\frac{1}{N_{fL}} + \frac{1}{N_{fS}}\right] + H_f\left(\frac{t_b}{2} - \frac{t_t}{2}\right) \tag{3.18}$$

Figure 3.3 shows the visual definition of the variables from Briggs and Young's (1963) correlation. Next, the heat transfer coefficient across the tube bundle can be solved for:

$$h_a = \frac{Nu_a k_a}{D_o} \tag{3.19}$$

3.2.3. Overall Heat Transfer Coefficient

The overall heat transfer coefficient is calculated using the internal and external heat transfer coefficients as well as the fin efficiency. The fin efficiency equation is derived in Appendix B. Using the derived equation, the cold side fin efficiency can be calculated. As there are no fins on the hot side, the hot side fin efficiency is assumed to be 1. The equation for the overall heat transfer coefficient is presented as

$$U_h = \left[\frac{1}{\eta_h h_{TP}} + \frac{\log(D_o/D_i)A_h}{2k_{st}L} + \frac{A_h}{\eta_c h_a A_c}\right]^{-1} \tag{3.20}$$

where η_h and η_c are the hot and cold side fin efficiencies respectively, k_{st} is the thermal conductivity of the steel, and the hot and cold side areas are defined as

$$A_h = D_i \pi L$$

$$A_c = \pi D_o(L - N_f t_b) + N_f L \left[2\pi \left(\frac{{D_f}^2}{2} - \frac{{D_o}^2}{2}\right) + t_t D_f \pi\right]$$

Then, the actual condenser capacity can be solved for using equation 3.3 for the hot side. This gives the equation

$$q_c = U_h A_h \Delta T_{lm} \tag{3.21}$$

3.3. Numerical Model

A numerical model is created in ANSYS Fluent (2013a) to provide another method to calculate the heat transfer coefficient across the tube bundle. First, a 2D model of the standard case of a flow across a cylinder is created to verify the solution method. Then a 3D model is created for a section of the ACC tube bundle. This section discusses the theory behind the calculation in ANSYS Fluent (2013a) and the calculations performed to support the numerical model.

3.3.1. Navier-Stokes Equations

The continuity equation, also known as conservation of mass, is written as

$$\frac{\partial \rho}{\partial t} + \nabla \cdot (\rho \vec{\mathrm{v}}) = 0 \tag{3.22}$$

The airflow across the tube bundle is assumed to be incompressible, making the density of the air a constant. Therefore, the continuity equation reduces to

$$\nabla \cdot \vec{\mathrm{v}} = 0 \tag{3.23}$$

Then, the momentum equation for incompressible flow is generally expressed as

$$\frac{\partial \vec{\mathrm{v}}}{\partial t} + (\vec{\mathrm{v}} \cdot \nabla)\vec{\mathrm{v}} = -\frac{1}{\rho}\nabla p + \nu \nabla^2 \vec{\mathrm{v}} + \vec{F} \tag{3.24}$$

where ρ is density, ν is the kinematic viscosity, p is pressure, and F represents body forces (Rutherford, 1989). The 2D and 3D numerical models are very similar, but the 2D model only considers two coordinates. For the 3D model, the z-direction is added.

3.3.2. Energy Equation

The energy equation accounts for conservation of energy within the system. The energy equation for the fluid region is defined as

$$\frac{\partial}{\partial t}(\rho h) + \nabla \cdot (\rho h \vec{v}) = \nabla \cdot [(k + k_t)\nabla T] \tag{3.25}$$

with k as the molecular conductivity and k_t as conductivity due to turbulent transport written as

$$k_t = \frac{C_p \mu_t}{Pr_t} \tag{3.26}$$

Additionally, h is the sensible enthalpy defined as

$$h = \int_{T_{ref}}^{T} C_p \mathrm{d}T \tag{3.27}$$

where T_{ref} is defined as 298.15 K.

3.3.3. k-ω SST Turbulence Model

In order to accurately model the turbulent crossflow over the tube bundle, the k-ω shear stress transport (SST) turbulence model is utilized in ANSYS Fluent (2013a). This two equation eddy-viscosity model is based on the original k-ω turbulence model developed by Wilcox and Rubesin (1980). With respect to accuracy and robustness, the k-ω model is one of the best available. The model solves for the turbulent kinetic energy, k, and the specific dissipation rate, ω (Menter, 1993) where ω is defined as

$$\omega = \frac{\epsilon}{k} \tag{3.28}$$

The SST model is a variation of this model that accounts for the main turbulent shear stress present in adverse pressure gradient boundary layers (Menter, 1993). The model is identical to the Wilcox and Rubesin (1980) model in the inner half of the boundary layer, then it gradually converts to the standard k-ϵ model closer to the boundary layer edge. The derivative allows for the calculation of transient changes in the flow field at each fixed point. The altered k-ω model holds on to the robustness and accuracy of the model developed by Wilcox and Rubesin (1980), while utilizing the "freestream independence" of the k-ϵ model (Menter, 1993). The altered equations for k and ω are respectively stated as:

$$\frac{D\rho k}{Dt} = \tau_{ij}\frac{\partial u_i}{\partial x_j} - \beta^* \rho \omega k + \frac{\partial}{\partial x_j}\left[(\mu + \sigma_k \mu_t)\frac{\partial k}{\partial x_j}\right] \tag{3.29}$$

$$\frac{D\rho\omega}{Dt} = \frac{\gamma}{\nu_j}\tau_{ij}\frac{\partial u_i}{\partial x_j} - \beta\rho\omega^2 + \frac{\partial}{\partial x_j}\left[(\mu + \sigma_\omega\mu_t)\frac{\partial\omega}{\partial x_j}\right] + 2(1-F_1)\rho\sigma_{\omega 2}\frac{1}{\omega}\frac{\partial k}{\partial x_j}\frac{\partial\omega}{\partial x_j} \quad (3.30)$$

The function F_1 is designed for near the wall, where the SST model is applied. Therefore blending will take place in the wake region of the boundary layer (Menter, 1993). The constant ϕ of the model is calculated from the constants ϕ_1 and ϕ_2

$$\phi = F_1\phi_1 + (1-F_1)\phi_2 \quad (3.31)$$

The ϕ_1 constants of the k-ω model are (Menter, 1993): $\sigma_k 1 = 0.85$, $\sigma_{\omega 1} = 0.5$, $\beta_1 = 0.075$, $\alpha_1 = 0.31$, $\beta^* = 0.09$, $\kappa = 0.41$, $\gamma_1 = \beta_1/\beta^*\text{-}\sigma_{\omega 1}\kappa^2/\sqrt{\beta^*}$, and the ϕ_2 constants of the transformed k-ϵ model are based on the standard k-ϵ model constants (Ferziger and Peric, 2002): $\sigma_k 2 = 1.0$, $\sigma_{\omega 2} = 0.856$, $\beta_2 = 0.0828$, $\beta^* = 0.09$, $\kappa = 0.41$, $\gamma_2 = \beta_2/\beta^*\text{-}\sigma_{\omega 2}\kappa^2/\sqrt{\beta^*}$. Next, the function F_1 is given as

$$F_1 = \tanh(a_1^4) \quad (3.32)$$

where a_1 is defined as

$$a_1 = \min\left(\max\left(\frac{\sqrt{k}}{0.09\omega y}; \frac{500\nu}{y^2\omega}\right); \frac{4\rho\sigma_{\omega 2}k}{CD_{k\omega}y^2}\right) \quad (3.33)$$

with y as the distance to the next surface and $CD_{k\omega}$ as the cross-diffusion term of equation 3.30

$$CD_{k\omega} = \max\left(2\rho\sigma_{\omega 2}\frac{1}{\omega}\frac{\partial k}{\partial x_j}\frac{\partial\omega}{\partial x_j}, 10^{-20}\right) \quad (3.34)$$

The SST model accounts for the turbulent stress tensor $\tau_{ij} = -\rho\overline{u'\nu'}$ to include the effect of the transport of the main turbulent shear stress. The following term is then included

$$\frac{Dr}{Dt} = \frac{\partial r}{\partial t} + u_k\frac{\partial r}{\partial x_k} \quad (3.35)$$

The transport equation for the turbulent shear stress τ is used from the turbulence model developed by Johnson and King (1985) and leads to the eddy-viscosity term defined by Menter (1993).

$$\nu_t = \frac{\alpha_1 k}{\max(\alpha_1\omega; \Omega F_2)} \quad (3.36)$$

where Ω is the absolute value of the vorticity and F_2 is defined as

$$F_2 = \tanh(a_2^2) \quad (3.37)$$

with

$$a_2 = max\left(2\frac{\sqrt{k}}{0.09\omega y}; \frac{500\nu}{y^2\omega}\right) \quad (3.38)$$

This modification of the eddy-viscosity has the largest impact on the boundary layer wake region (Menter, 1993).

Turbulence parameters are then defined by simple calculations. The turbulence intensity is defined as

$$I = \frac{u'}{u_{avg}} \tag{3.39}$$

and the turbulent viscosity ratio, $\frac{\mu_t}{\mu}$, can range from 0.1-1 for external flows. (ANSYS Fluent, 2013c).

3.3.4. Cylinder in Crossflow

A 2D model is created for a simple geometry of a cylinder in crossflow. The geometry created is shown in figure 3.5. The cylinder outline is the circle and the rectangle represents the flowfield. The geometry size is a function of the cylinder radius, where the length from the cylinder's center to the inlet is 50 times the radius. This distance allows for the flow to be properly introduced to the control volume. The distance to the top and bottom is half the distance to the inlet and outlet. Figure 3.5 also shows the boundary conditions assigned to each boundary.

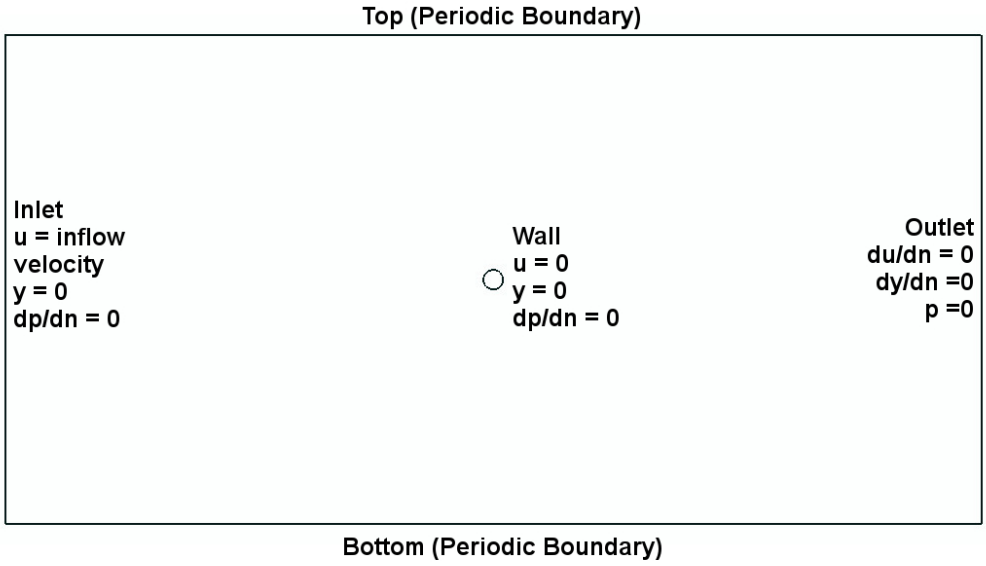

Figure 3.5: 2D geometry and boundary conditions of cylinder in crossflow

The left hand side represents the inlet, where a constant value is applied to the inflow velocity (u). The right hand side is the flow outlet, defined as a pressure outlet with zero gauge pressure. The top and bottom boundaries are defined as periodic boundaries, where the two boundaries are paired. Therefore, the flow entering the

bottom is periodically repeated leaving the top boundary. The periodic boundary is defined as a translational periodic boundary. Additionally, the front and back sides of the model (fin side and tube side) have symmetric conditions.

In order to perform a calculation for this field a mesh is generated using GMSH (2014). The mesh is refined around the edge of the cylinder in order allow for precise calculations in the boundary layer. The refinement around the cylinder wall is shown in figure 3.6 along with the tube wall boundary. The "no slip" condition represents a zero velocity at the wall, assuming a viscous fluid with a shear force. In order to correctly represent the velocity profile around the cylinder, standard wall functions are applied.

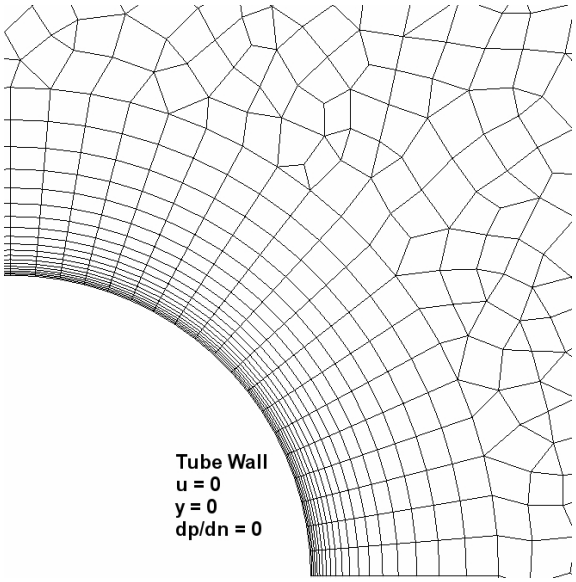

Figure 3.6: 2D model mesh refinement is gradual around the cylinder wall

The measure of a good mesh is the value of y^+, the non-dimensional wall distance for a wall-bounded flow. The value is defined by the following equation

$$y^+ = \frac{u^* y}{\nu} \tag{3.40}$$

where y is the distance to the nearest wall, ν is the kinematic viscosity of the fluid, and the friction velocity, u^*, is defined as

$$u^* = \sqrt{\frac{\tau}{\rho}} \tag{3.41}$$

where τ is wall shear stress. In the viscous sublayer, the y^+ value should be less than five but it is preferable to reach below a value of one (Pope, 2000). Therefore, it is essential to calculate the $y+$ value for each mesh generated.

Dimensionless Groups

In order to analyze the flow, three dimensionless parameters are used; Nusselt number (Nu), Strouhal number (Sr) and coefficient of drag (C_d). Just as in the analytical model, the Reynolds number is defined as

$$Re = \frac{D_o u_a}{\rho_a} \tag{3.42}$$

where u_a is the fixed inlet air velocity and D_o is the outer diameter of the cylinder. This velocity and Reynolds number stay constant throughout the whole problem. Then, the Nusselt number is defined as

$$Nu = \frac{h_a D_o}{k_a} \tag{3.43}$$

where k_a is the thermal conductivity of air. In this case the heat transfer coefficient is not known, therefore another equation is needed to solve for the Nusselt number. A general heat transfer equation can be written:

$$q = h_a A(T_w - T_{ci}) \tag{3.44}$$

where A is the circumference of the cylinder multiplied by a unit length. Therefore, by inserting equation 3.44 into equation 3.43, the equation for the Nusselt number becomes

$$Nu = \frac{q}{\pi k_a (T_w - T_{ci})} \tag{3.45}$$

Next, the Strouhal number is defined as

$$Sr = \frac{fD}{u_a} \tag{3.46}$$

with frequency, f, defined as

$$f = \frac{1}{T} \tag{3.47}$$

where T is the time period of the variation in coefficient of lift (C_l).

ANSYS Fluent (2013a) can write the coefficient of lift (C_l) and coefficient of drag (C_d) to separate ASCII files. From there, the period (T) can be obtained to calculate the Strouhal number. Similarly, the average coefficient of drag can be calculated from the file.

3.3.5. Tube Bundle in Crossflow

When creating the 3D model of the tube bundle it is important to choose a section of the bundle that adequately describes the flow traveling through the bundle. The section being analyzed in this model is shown as dashed lines in figure 3.7.

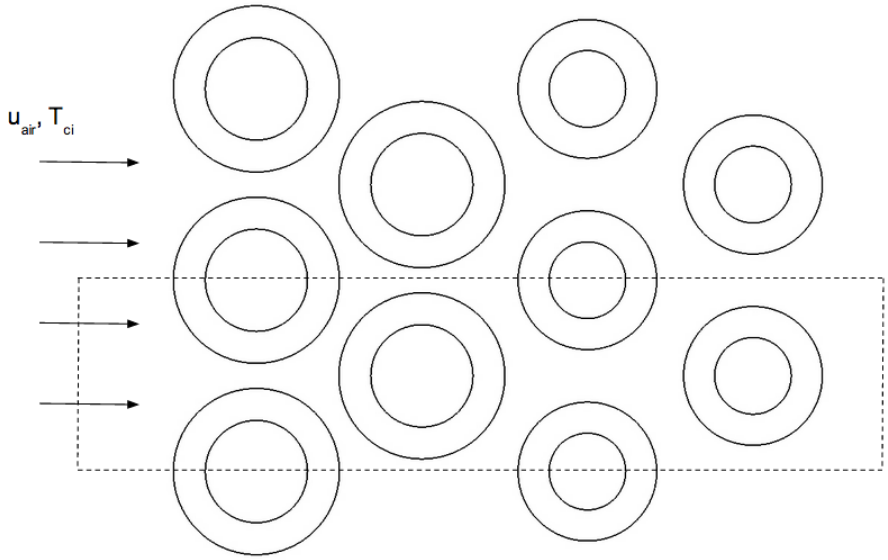

Figure 3.7: A section of the tube bundle front is analyzed in the model

Additionally, the side view section needs to be carefully chosen. As shown by the dashed lines in figure 3.8, the section being analyzed in this model is from the edge of one fin to half the distance between two fins. Therefore the model will account for a fin wall on one side and air across a tube on the other side. It is to be noted that figure 3.8 is not drawn to scale, it is solely for visual explanation purposes.

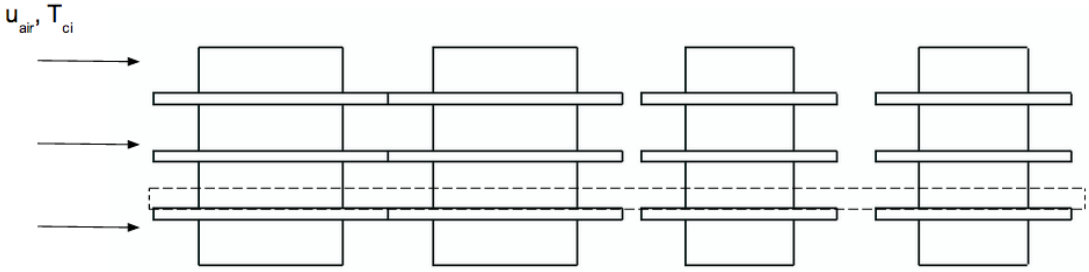

Figure 3.8: A section of the tube bundle side is analyzed in the model

When modeling this flow it is assumed that the fins are infinitely thin. Thus, the air flow at the inlet is a constant velocity value. This will have some affect on the accuracy of the model, but the error should be minimal. Additionally, a fin and tube wall temperature is assigned as a constant value.

The geometry of the 3D model is then sketched and boundary conditions are applied, which can be seen in figure 3.9. As seen in the figure, the boundary conditions for the tube bundle are similar to those stated for the 2D model of a cylinder in crossflow. Furthermore, the front and back sides of the geometry (each side of the z-direction) are defined as symmetries to account for the tube and fin located above and below. In addition the fin wall is labeled as a "wall", just as the tube wall. The

fin wall is outlined in red in the figure. As the mesh is so small in the z-direction, a side view will not be displayed. Just as in the 2D model, the y^+ value should be checked for both the fin and the tube wall. By using a similar Reynolds number as in a verified 2D model, it can be expected to get results of the same accuracy for the 3D model.

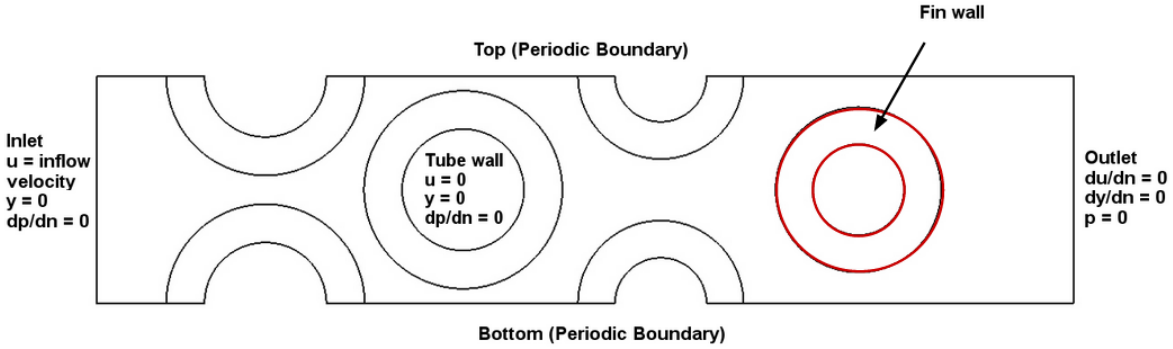

Figure 3.9: The 3D model boundary conditions are similar to the 2D model

A 3D mesh is generated for the geometry using a similar refinement as is used around the tube and fin walls in the 2D model. Therefore, the two meshes should result in similar calculation accuracies. Figure 3.10 shows a zoomed view of the refinement in the 3D model.

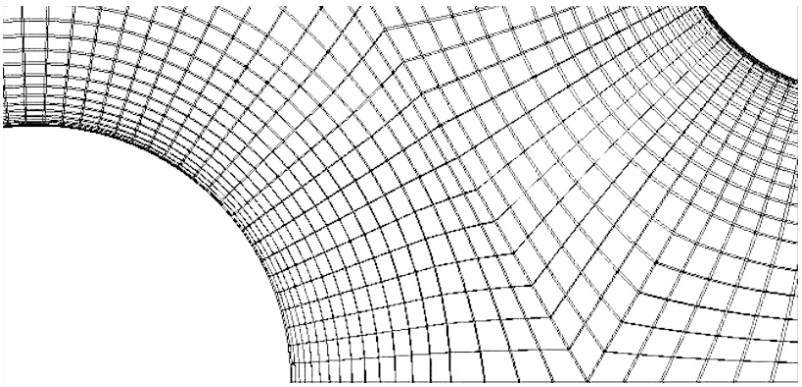

Figure 3.10: A zoomed view of the 3D mesh shows gradual refinement

In order to calculate the total heat transfer coefficient across the tube bundle, the following equation is used

$$h = \frac{q_{net}}{A(T_w - T_{in})} \tag{3.48}$$

where q_{net} is the total heat transfer from the tube and fin walls, and A is the total fin and tube wall area in the flowfield.

3.3.6. Simulation Setup

In order to solve the problem, a pressure based solver is used. The Pressure-Implicit with Splitting of Operators (PISO) solver is a part of the SIMPLE family of algorithms, however, it is mainly based on the relation between the corrections for pressure and velocity. The solver uses two additional corrections; the neighbor correction and skewness correction (ANSYS Fluent, 2013b). Additionally, the PISO algorithm allows for the use of large time steps as it can maintain a stable calculation.

The time step for the 2D model is calculated from the estimated Strouhal number for the cylinder, using the following equation

$$T = \frac{D_o}{Sr\ u_a n_{cycle}} \tag{3.49}$$

where n_{cycle} is the number of time steps per cycle and u_a is the inlet air velocity. Maximum time steps per cycle is set at 20 by default, and it is kept as is. A simulation for the 2D case should be run until the coefficient of lift has reached a steady state. The velocity value to be used in this case is the same as is calculated in the analytical model. This is done in order to evaluate how the two models differ. The 3D tube bundle case is kept very similar. For the 3D case it can be assumed that a flow that passes five times thorough the bundle is sufficient for the calculation. A good measure of the simulation quality is the dimensionless transport per time step, or Courant number, defined as

$$\alpha = \frac{u\Delta t}{\Delta x} \tag{3.50}$$

where u is the local flow velocity, Δt is change in time, and Δx is change in location. The Courant number for the 3D flow should be low for improved accuracy.

4. Results

This chapter discusses the main results from both the analytical and numerical model. Furthermore, a mesh convergence study is performed for each numerical model; 2D and 3D. The results for the analytical and numerical models are also compared to the GEA data.

4.1. Analytical Model

The analytical model calculates the total areas for both sides. The volumetric flow rate given by GEA as 805.6 m^3/s is used to calculate the face velocity for this ACC unit. The face velocity is calculated to be 1.79 m/s, a bit lower than the 1.95 m/s from the GEA data. This error can be related to the area calculation, as it is not known where the fins start on the tube. The fin efficiency is calculated to be 95 %, therefore the fin and tube wall temperatures are assumed to be the same, and are assigned a constant value of 318.92 K. The inlet air temperature is also assigned a constant value of 293 K. Next the face velocity is used to calculate the heat transfer coefficient across the bundle, the overall heat transfer coefficient and the cooling capacity of the ACC. Furthermore, the total condenser cooling requirement is calculated for the system as 14.6 MW. However, as seen in table 4.1 the calculated cooling capacity of the ACC is 13.9 MW.

Table 4.1: Analytical model results are clear

Variable	**Analytical Model**
h_a [W/m^2K]	19.9
U_h [W/m^2K]	396.0
q_c [MW]	13.89

The results from the analytical model will later be compared with the numerical model results.

4.2. Numerical Model

The numerical model results are split into their two respective sections; cylinder in crossflow and tube bundle. The two model results are analyzed in this section.

4.2.1. Cylinder in Crossflow

The 2D problem is first solved using information from literature. Three non-dimensional parameters are used for flow comparison; Nusselt number (Nu), Strouhal number (Sr) and coefficient of drag (C_d). The two-phase heat transfer coefficient calculated in the analytical model is applied to the numerical model. Additionally, from the analytical model, the face velocity is 1.79 m/s, therefore the Reynolds number for this flow is just under 5700. From the research conducted by Roshko (1954) and Jones (1968) the Strouhal number should range from 0.18 to 0.21. Additionally, when then the Nusselt number is calculated using the correlation developed by Churchill and Bernstein (1977), the value is 40.26. However, using graphical representation developed from the studies by Knudsen and Katz (1958), and Hilpert (1933) the number can range from 40-50. Therefore, it can be assumed that the Nusselt number should fall in the range of 40-50. Furthermore, the coefficient of drag should be close to 0.9 (Schlichting, 2000).

Mesh Convergence Study

The 2D mesh is created in three different refinements; coarse, medium, and fine. This allows for a mesh convergence study to be performed. The number of cells corresponding to each refinement is listed in table 4.2.

Table 4.2: Number of cells corresponding to various 2D mesh refinements

Mesh	**Number of cells**	**Increase [%]**
Coarse	76358	-
Medium	118802	55.59
Fine	177251	132

As seen in the table, the difference between the finest mesh and the one most coarse is 132%. The mesh refinement should be sufficient to capture the flow characteristics. In order to evaluate the quality of each mesh, the y^+ value is analyzed. The y^+ value

for this cylinder is set to 1.01 for all mesh refinements.

Next, a simulation is run for each of the mesh refinements until the coefficient of lift shows steadiness. The computation solves a total of 10 seconds of the flow for each mesh. The plot for the finest mesh can be seen in figure 4.1.

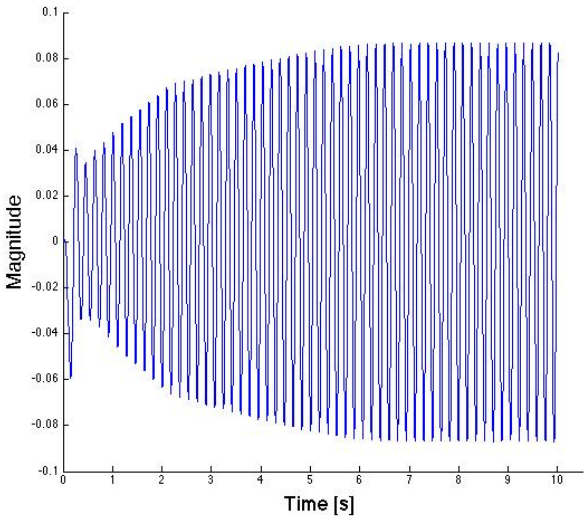

Figure 4.1: Coefficient of lift plotted agains simulation time

From figure 4.1 the period of the wave is measured to calculate the Strouhal number for the cylinder. Additionally, the coefficient of drag is plotted against time in order to find its value. Finally, the other dimensionless parameters are calculated. All three parameters are compared for each simulation in order to see if the meshes are converging. The results are listed in table 4.3.

Table 4.3: Mesh convergence study for the 2D model

Mesh	**Nu**	**Sr**	**Cd**
Coarse	33.504	0.161	0.837
Medium	46.056	0.166	0.873
Fine	45.655	0.167	0.855

From table 4.3, it is clear that the solution is not deviating greatly from the medium to fine mesh refinement. It is also evident that the mesh is converging when the cell number is increased. Therefore it can be assumed that the medium mesh is sufficient for further calculations.

Simulation Results

The medium mesh values are used for a simple comparison between values obtained from literature and the results of the 2D mesh. The two are paired up in table 4.4. As the literature stated a range for the Nusselt number and Strouhal number, the calculated Nusselt number and the median of the Strouhal range are used for comparison. In order to understand how accurate the model is, the relative error is calculated using the following equation

$$\epsilon_{rel} = \frac{|x_i - x_{actual}|}{x_{actual}} \tag{4.1}$$

where x_i is the value obtained from the numerical model and x_{actual} is the value obtained from literature. Table 4.4 also shows the relative error for each dimensionless parameter.

Table 4.4: 2D model results are compared to literature

Variable	**Literature**	**2D Model**	$\epsilon_{\mathbf{rel}}$ **[%]**
Nu	40.26	46.056	12.58
Sr	0.195	0.166	14.87
C_d	0.9	0.873	3

Table 4.4 shows that the 2D model sufficiently represents the crossflow across the cylinder. An error up to 15 % can be expected from this model using ANSYS Fluent (2013a). Using a similar Reynolds number, a 3D model with the same case setup should result in similar error. A contour plot of the 2D velocity profile of the fine mesh can be seen in figure 4.2.

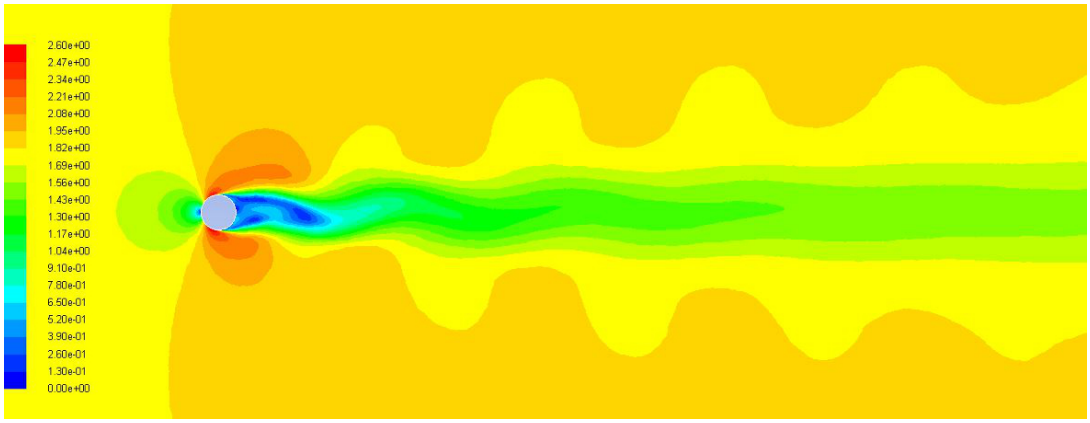

Figure 4.2: Zoomed-in velocity contour of the cylinder in crossflow

As seen in the image, the vortex shedding clearly appears in the flowfield, as expected.

4.2.2. Tube bundle

The tube bundle mesh is generated in three different refinements; coarse, medium, and fine. Just as with the 2D model, this is done in order to perform a mesh convergence study. The number of cells corresponding to each mesh refinement is shown in table 4.5.

Table 4.5: Number of cells corresponding to various 3D mesh refinements

Mesh	**Number of cells**	**Increase [%]**
Coarse	79500	-
Medium	119250	50
Fine	477000	500

The 3D model of the tube bundle is set up similarly to the 2D model. As seen in the table, the fine mesh is very refined which will lead to a much longer computation time. The flow is solved for a time that allows the air to pass five times through the solution domain with a Courant number of seven. At the inlet the turbulence intensity, I, is assigned the calculated value of 5 % and the turbulent viscosity ratio is 0.1.

Mesh Convergence Study

The 3D tube bundle mesh also needs to be evaluated, thus the y^+ value is analyzed. The y^+ value for the bundle is listed in table 4.6 for all mesh refinements, where the y^+ value listed is the largest value obtained around the fin and tube walls.

Table 4.6: Values of y^+ for the 3D model

Mesh	**y^+ of fin**	**y^+ of tube**
Coarse	0.96	3.87
Medium	0.77	3.68
Fine	0.48	1.61

The y^+ values for the tube bundle are also within the desired limits, below five, or close to one. Thus, the solution should be an accurate representation of the flow. A mesh convergence study is also performed for the 3D model, shown in table 4.7. The three variables chosen are the heat transfer coefficient (h_a), the mean temperature at tube bundle outlet (T_{co}), and the total forces on all tubes and fins combined.

Table 4.7: Mesh convergence study for the 3D model

Mesh	**h_a [W/m^{2}K]**	**T_{co} [K]**	**Total forces [mN]**
Coarse	17.92	309.54	3.772
Medium	17.99	310.01	3.769
Fine	17.69	308.52	3.788

The heat transfer value stays fairly constant for all three meshes, thus the meshes converge. The results of this simulation should be a fair representation of the actual air flow and heat transfer. Therefore, the medium mesh results can be used to calculate the hot side overall heat transfer coefficient and the cooling capacity of the ACC. In order to improve accuracy, the Courant number is lowered to a value of three. Despite the lowered Courant number, the results do not change greatly. Therefore, the model is showing good convergence and does not need to be further refined.

Simulation Results

Figures 4.3 and 4.4 show the temperature profile for both the front and back of the model. The front corresponds to the location between two fins, whereas the back side represents the location flush with the fins. The temperature profile shows how the air enters the bundle at 293 K and heats up as it passes through. Then it exits the bundle at an average of 308 K.

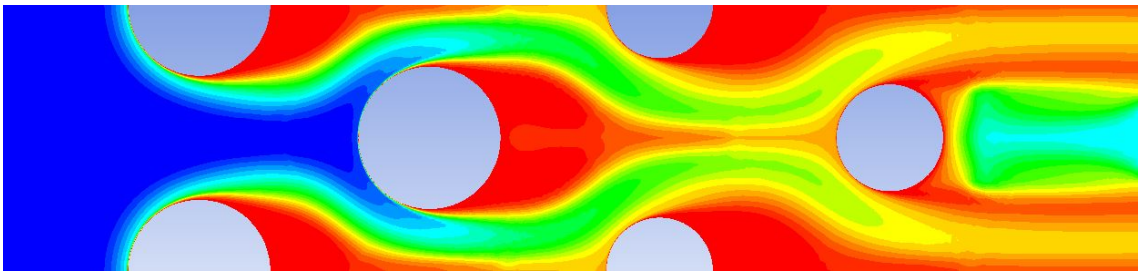

Figure 4.3: Front side (tube) temperature profile of the tube bundle

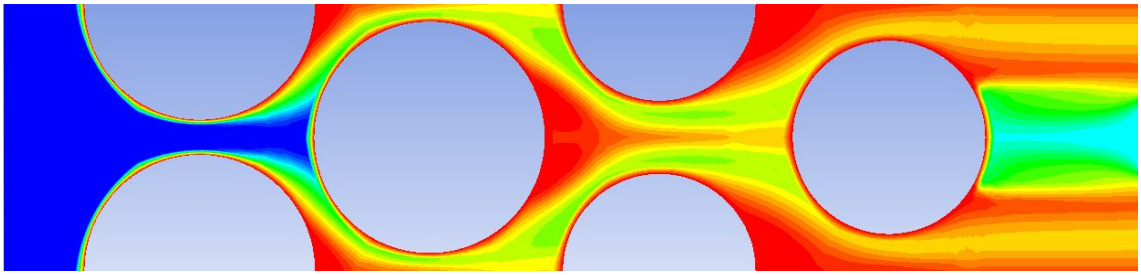

Figure 4.4: Back side (fin) temperature profile of the tube bundle

Similarly, the velocity profile for both the back and front sides of the model are generated. The velocity profile of the front and back can be seen in figures 4.5 and 4.6, respectively.

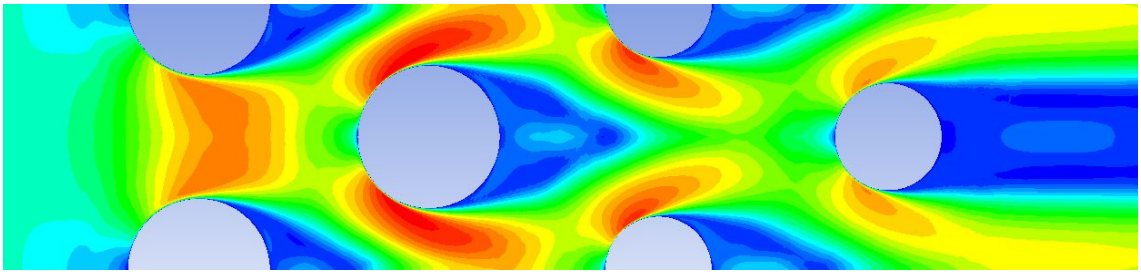

Figure 4.5: Front side (tube) velocity profile of the tube bundle

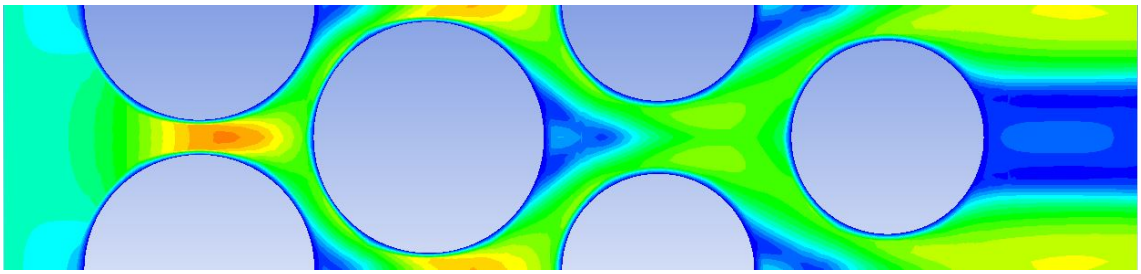

Figure 4.6: Back side (fin) velocity profile of the tube bundle

The velocity profile shows the air entering at 1.79 m/s and speeding up as it passes through the small openings between tubes. The turbulent intensity is also

plotted for the model and the front and back profiles can be seen in figures 4.7 and 4.8

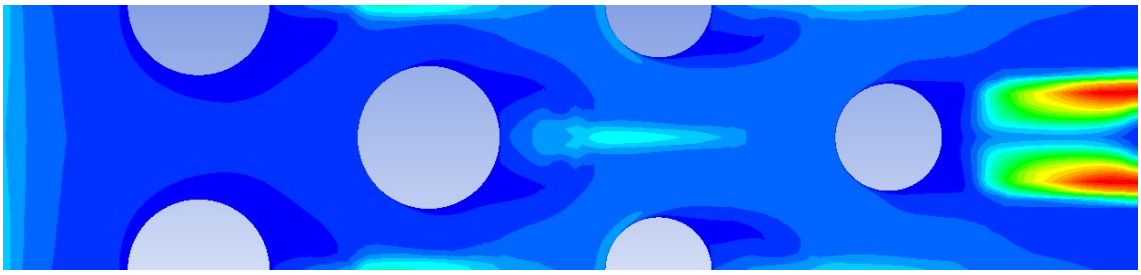

Figure 4.7: Front side (tube) turbulent intensity profile of the tube bundle

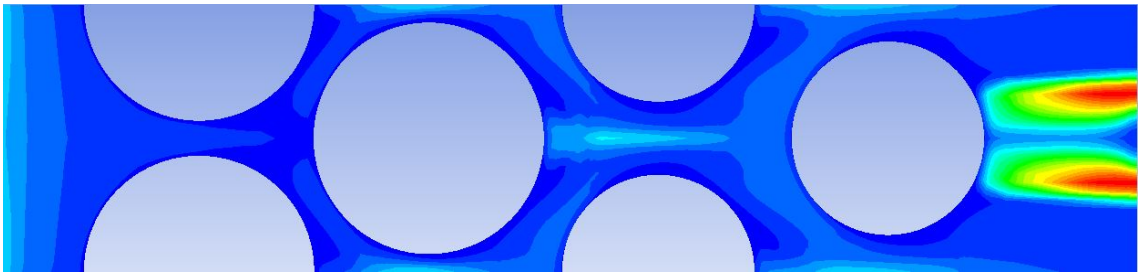

Figure 4.8: Back side (fin) turbulent intensity profile of the tube bundle

The results from the simulation are further analyzed where the heat transfer coefficient is used to calculate the hot side overall heat transfer coefficient and the total cooling capacity of the ACC. The information is listed in table 4.8.

Table 4.8: Tube bundle model results

Variable	**Numerical Model**
h_a [W/m^{2}K]	18.0
U_h [W/m^{2}K]	374.7
q_c [MW]	13.15

The results from the numerical model will then be compared with the analytical model results. Additionally, both results need to be compared with the original data provided by GEA.

4.3. Model Comparison and Discussion

The models provide two different tools for solving for the heat transfer coefficient across the tube bundle. When taking a look at the results from the two models listed in table 4.9, it is evident that both deviate from the original data provided by GEA.

Table 4.9: Model results

	GEA Data	**Analytical Model**	**Numerical Model**
h_a [W/m^{2}K]	21.5	19.9	18.0
U_h [W/m^{2}K]	390.8	396.0	374.7
q_c [MW]	13.86	13.89	13.15

Looking at the table, it is evident that the numerical model deviates more from the GEA data than the analytical model. The deviation from the GEA data can be a result of an inaccurate area calculation for the tube bundle. The inlet velocity calculated in the analytical model is 1.79 m/s, but the GEA data sheet states that it is 1.95 m/s. It is not known exactly how long the tubes stick out on each side of the fins located on the edge. Therefore, that slight bit of unknown area might need to be more accurately accounted for when calculating the total face area. Additionally, the thin fin assumption can impact the solution. Therefore, the error can either lie in the area calculation or infinitely thin fin assumption.

As expected from the 2D model calculations, the error in the heat transfer coefficient calculation can be up to 15 %. Therefore, it is known that the numerical model will lead to a less accurate solution. The cooling capacity of the ACC calculated using the analytical model is only at a 0.3 % relative error from the GEA data. The numerical model, however, results in a lower cooling capacity within a 5 % relative error. This shows that both models are providing good results, but the analytical model is more accurate.

5. Conclusion

A geothermal power plant that uses an air cooled condenser to condense the steam is a system that solves the problem of extensive cold water usage in water cooled power plants. Additionally, it eliminates the vapor plume visible in power plants that are coupled with a cooling tower. Therefore, the air cooled system is one that is environmentally sound and worth a closer look.

An extensive literature review is performed to gain knowledge about the correlations available for calculating the internal and external heat transfer coefficients of tube flow. Next, two correlations are chosen to represent the air cooled condenser flow; the correlation of condensation inside tubes developed by Chato (1960), and the correlation for a staggered tube bundle in crossflow developed by Briggs and Young (1963). The two models created for the study are the analytical and numerical models. The standard case of a flow across a cylinder in 2D results in a 15 % error. Therefore, a 15 % error is expected from the numerical model. However, when compared, the condenser cooling capacity errors are 5 % and 0.3 % for the numerical and analytical models respectively. Neither error is significant and both models can be used when designing an ACC unit. However, the more accurate solution for the air flow heat transfer coefficient is obtained by the Briggs and Young (1963) correlation, as was done in the analytical model.

The next steps for this study could be to investigate the effect of the different sized tube diameters. Another simulation in ANSYS Fluent (2013a) can show how the heat transfer coefficient changes if the tube diameters are all the same size. It would also be interesting to further investigate how the staggered tube arrangement affects the heat transfer coefficient. It would be expected that the staggered arrangement increases the heat transfer coefficient, however, it is interesting to analyze this. Furthermore, using a plate-finned tube bundle instead of the annular fins is another arrangement that can be investigated for the heat transfer coefficient variation.

The practical usage of this study can then be highlighted. When designing an ACC unit, the correlation developed by Briggs and Young (1963) will lead to an accurate representation of the airflow. Additionally, the correlation developed by Chato (1960) results in accuracy regarding the internal flow. These two correlations can then be used to aid the ACC design where accurate results are expected. The numerical model suits better if a visual representation of the airflow is desired. The two models can be used in order to optimize an air cooled condenser design by altering the number of tube rows, tube diameter or total number of tubes.

Bibliography

Akhavan-Behabadi, M., Kumar, R., and Mohseni, S. (2007). Condensation heat transfer of R-134a inside a microfin tube with different tube inclinations. *International Journal of Heat and Mass Transfer*, *50*.

ANSYS Fluent, A. R. (2013a). Release 14.5.

ANSYS Fluent, A. R. (2013b). Release 14.5, Theory Guide: PISO.

ANSYS Fluent, A. R. (2013c). Release 14.5, User's Guide: Determining Turbulence Parameters.

Briggs, D., and Young, E. (1963). Convective Heat Transfer and Pressure Drop of Air Flowing Across Triangular Pitch Banks of Finned Tubes. *Chemical Engineering Progress Symposium Series*, *59*(41), 1–10.

Caruso, G., and Vitale Di Maio, D. (2013). Heat and mass transfer analogy applied to condensation in the presence of noncondensable gases inside inclined tubes. *International Journal of Heat and Mass Transfer*, *68*.

Caruso, G., Vitale Di Maio, D., and Naviglio, A. (2013). Film condensation in inclined tubes with noncondensable gases: An experimental study on the local heat transfer coefficient. *International Communications in Heat and Mass Transfer*, *45*.

Chato, J. (1960). *Laminar Condensation inside Horizontal and Inclined Tubes*. Ph.D. Thesis, Massachusetts Institute of Technology, Massachusettes, USA.

Chiou, J., Yang, S., and Chen, C. (1994). Laminar film condensation inside a horizontal elliptical tube. *Applied Mathematical Modelling*, *18*.

Churchill, S., and Bernstein, M. (1977). A Correlating Eequation for Forced Convection from Gases and Liquids to a Circular Cylinder in Crossflow. *Journal of Heat Transfer*, *99*.

Conradie, A., and Kröger, D. (1996). Performance Evaluation of Dry-Cooling Systems for Power Plant Applications. *Applied Thermal Engineering*, *16*(3), 219–232.

Ferziger, J., and Peric, M. (2002). *Computational Methods for Fluid Dynamics*. Berlin, Germany: Springer-Verlag, 3 ed.

GMSH (2014). C. Geuzaine and J.-F. Remacle. Gmsh: a three-dimensional finite element mesh generator with built-in pre- and post-processing facilities. Version 2.8.4.

Gray, D., and Webb, R. (1986). Heat Transfer and Friction Correlations for Plate Finned-Tube Heat Exchangers Having Plain Fins. *International Journal of Heat and Mass Transfer*, *8*.

Green Energy Group (2014). Green Energy Group: Power From Within.

Hilpert, R. (1933). Wärmeabgabe von geheizen Drahten und Rohren. *Forsch. Geb. Ingenieurwes*, *4*.

Hofmann, R., Frasz, F., and Ponweiser, K. (2007). Heat Transfer and Pressure Drop Performance Comparison of Finned-Tube Bundles in Forced Convection. *WSEAS Transactions of Heat and Mass Transfer*, *2*.

Hu, H., and Chen, C. (2005). Simplified approach of turbulent film condensation on an inclined elliptical tube. *International Journal of Heat and Mass Transfer*, *49*.

Johnson, D., and King, L. (1985). A Mathematically Simple Turbulence Closure Model for Attached and Separated Turbulent Boundary Layers. *AIAA Journal*, *23*.

Jones, G. W. J. (1968). Wind tunnel study of unsteady lift forces generated by vortex shedding about large, stationary, and oscillating cylinder at high reynolds numbers. *ASME Symp. Unsteady Flow*.

Kagel, A., Bates, D., and Gawell, K. (2007). A Guide to Geothermal Energy and the Environment. Tech. rep., Geothermal Energy Association, Washington, D.C., USA.

Kim, S., and No, H. (1999). Turbulent film condensation of high pressure steam in a vertical tube. *International Journal of Heat and Mass Transfer*, *43*.

Knudsen, J., and Katz, D. (1958). *Fluid Dynamics and Heat Transfer*. New York, USA: McGraw-Hill.

Kristmannsdóttir, H., and Ármannsson, H. (2003). Environmental aspects of geothermal energy utilization. *Geothermics*, *32*, 451–461.

Lips, S., and Meyer, J. (2011a). Experimental study of convective condensation in an inclined smooth tube. Part I: Inclination effect on flow pattern and heat transfer coefficient. *International Journal of Heat and Mass Transfer*, *55*.

Lips, S., and Meyer, J. (2011b). Experimental study of convective condensation in an inclined smooth tube. Part II: Inclination effect on pressure drops and void fractions. *International Journal of Heat and Mass Transfer*, *55*.

Lips, S., and Meyer, J. (2011c). Two-phase flow in inclined tubes with specific reference to condensation: A review. *International Journal of Multiphase Flow*, *37*.

Lips, S., and Meyer, J. (2012). Stratified flow model for convective condensation in an inclined tube. *International Journal of Heat and Fluid Flow*, *36*.

MATLAB, T. M. I. (2013). version 8.1.0.604 (R2013a).

Menter, F. R. (1993). Zonal Two Equation k-ω Turbulence Models for Aerodynamic Flows. *AIAA Paper 93-2906*.

Meyer, J., Dirker, J., and Adelaja, A. (2013). Condensation heat transfer in smooth inclined tubes for R134a at different saturation temperatures. *International Journal of Heat and Mass Transfer*, *70*.

Mortensen, K. (2011). Improved Performance of an Air Cooled Condenser (ACC) Using SPX Wind Guide Technology at Coal-Based Thermoelectric Power Plants. Tech. rep., SPX Cooling Technologies, Inc.

Pope, S. (2000). *Turbulent Flows*. Cambridge, MA, USA: Cambridge University Press, 1 ed.

Roshko, A. (1954). On the development of turbulent wakes from vortex streets. *National Advisory Committee for Aeronautics*, *1191*.

Rutherford, A. (1989). *Vectors, Tensors, and the Basic Equations of Fluid Mechanics*. New York, USA: Dover Publications Inc.

Schlichting, H. (2000). *Boundary Layer Theory*. New York, USA: Springer.

Shah, M. (1979). A General Correlation for Heat Transfer During Film Condensation Inside Pipes. *International Journal of Heat and Mass Transfer*, *22*.

Wang, B., and Du, X. (1999). Study on laminar film-wise condensation for vapor flow in an inclined small/mini diameter tube. *International Journal of Heat and Mass Transfer*, *43*.

Wang, W., Ma, X., Wei, Z., and Yu, P. (1998). Two-phase flow patterns and transition characteristivs for in-tube condensation with different surface inclinations. *International Journal of Heat and Mass Transfer*, *41*.

Wilcox, D., and Rubesin, M. (1980). Progress in Turbulence Modeling for Complex Flow Fields Including the Effect of Compressibility. *NASA TP-1517*.

Würfel, R., Kreutzer, T., and Fratzscher, W. (2003). Turbulence Transfer Processes in Adiabatic and Condensing Film Flow in an Inclined Tube. *Chemical Engineering and Technology*, *26*.

Yazbek, W. (2013). Air Cooled Heat Eexchanger. GEA. Data sheet, unpublished raw data.

Zammit, K. (2005). Air-Cooled Condenser Design, Specification, and Operation Guidelines. Tech. rep., Electric Power Research Institute.

A. GEA Data

```
Rev| DATE     | BY | CHECK| FILE   |0        AIR COOLED HEAT EXCHANGER              |        GEA - BTT
 0 |          |    |      | 13570A |         ************************ version 12.0  | BATIGNOLLES Technologies Thermiques
 1 |19/08/13  | WY |      |--------|                                                |       *******************
 2 |          |    |      |  ITEM  | Customer        : GREEN ENERGY GROUP AS        | 25, rue du RANZAI - F 44300 NANTES
 3 |          |    |      |  ACC   | Plant Location  :                              |      Tel :(33)2.40.68.24.24
 4 |          |    |      |        | Service         : Air cooled condenser         |      Fax :(33)2.40.50.13.37

No of Units :  1        No of Bay/Unit      :  2
Selection   :2109-33. 4 Type: 1 FAMA        Draft :Forced

Surface/Unit...........Finned:              41651       m2
            ........Bare Tube:               2549       m2

Total Heat Exchanged  /  MTD :      13855      kW     / 15.5'C

              OVERALL HEAT TRANSFER RATE  :
Finned Tube                     :      21.52        W/m2.'C
Bare Tube , Service             :     351.70          "
Bare Tube , Clean               :     390.77          "

                         TUBE SIDE DATA
               ===========================
Fluid Circulated          :
Total Fluid Entering      :              25000.0        kg/h
                                 IN              OUT
  Temperature             :     45.1    |       43.0    'C
  Vapor                   :             |               kg/h
  Liquid                  :             |
  Steam                   :  21424.0    |      750.0     "
  Water                   :   3201.2    |    23875.0     "
  Noncondensable          :    375.0    |      375.0     "
  Vapor Mol.Wt.           :     18.0    |       18.0

Viscosity         V/L   : 0.011/  0.596|0.011/  0.610cP
Density           V/L   :  0.066/ 989.8|  0.064/ 990.4kg/m3
Specif. Heat      V/L   :  1.887/4.176 |  1.885/4.176 kJ/kg.'C
Thermal Conduct V/L     :  0.021/0.637 |0.021/0.636 W/m.'C
Enthalpy                        :         2273.7          kJ/kg
Pressure Out (Turbine)          :           0.100         BAR Abs.
Pressure In      (ACC )         :           0.097         BAR Abs.
Pressure Drop Allow./Calc.      :          / 0.003        BAR
Cleanliness factor              :           0.90

                          AIR SIDE DATA
               ===========================
Total Air Quantity              :      805.6    m3/s(20'C,1 atm.)
Air Quantity Per Fan            :      501.7    m3/s
Face Velocity                   :       1.95    m/s
Temperature  In/Out             :   20.0/ 34.2  'C
Actual Static Pressure          :      0.094    kPa
Altitude                        :      2010.    m
SPL at 1 m beside equipment     :       85      dB(A)


Weight Empty : 210700.   kg/Unit
```

```
                          CONSTRUCTION
                          ============
Design/Test Pressure     :   0.50+ F.V    / per code     BAR Eff.
Design Temperature       :  110.  'C
Construction Code     : ASME VIII DIV 1+ STD BTT
____________ BUNDLES ___________________  ___ HEADERS ____________
Size        :  3.52 m x 10.3 m          |Type :     ( 2 )
No/Bay      :    6                      |No Passes: 1       Split  : NO
No TOTAL    :   12                      |Pass Pattern:
No Tube Rows:    4                      |Nozzles In/Out     : 1x 56"/1x 3"
Frame       :  CARBON STEEL             |Rating      : BUTT WELD END
Slope       : "A" frame                 |Tube/Tubesheet   :STRENGTH WELD.
_______________ TUBES __________________|Header Mat.     : SA-240 GR316L
Material    :  SA-249 TP 316 L          |Gasket Mat.     :
Type        :  WELDED                   |Plug Mat.       :
Diameter    :  50.80 / 38.10   mm       |Corrosion Allowance   : 0.000 mm
Thickness   : 1.651   mm min.   (1)     |TI/PI Connect.: NO   / NO
No/Bundle   :  146    Total: 1752       |_________ MISCELLANEOUS _________
Length      :  10.000           m       |Structure   :   A        9.0m STEEL
Tri. Pitch:     95.00           mm      |Louvers     :         NO
________________ FINS __________________|Walkways    :HEAD. + MECHA.STEEL
Material    : ALUMINIUM                 |Fan Guards  :       STEEL
Diameter    :  82.55 / 69.85    mm      |Vibr.Switch:        IP55
No/Meter    :  354  / 394               |Steam Coils:        NO
Type        : EMBEDDED                  |

No/Bay      : 1         MECHANICAL EQUIPMENT            NO TOTAL  :  2
                      ======================
______________ FANS _______________________ ___ MOTORS ________________
Model      : (*)                          |Type: ELECTRIC    T.E.F.C.
Blades     : (*)              ALUMINIUM   |RPM               : 1500     RPM
kW / Fan                :       77.0 kW   |kW / Motor        :      90.0 kW
Tip Speed               :       44.0  m/s |Specials          :     415-3-50
Diameter                :        9.14  m  |_________ SPEED REDUCER _______
Pitch :         MANUAL. ADJUSTABLE        |Type:      GEAR
Pitch Angle             :       #         |Ratio             : 1475/ 92 = 16.00
Hub Mat. :          STEEL/ALU.            |Pulley Material :

(1)Under groove.
(2) Inlet header          : Manifold ø   56"
    Outlet headers        : Welded bonnets


(*)All data mentioned, partic. material and no. of blades are
 subject to modifications according to the selected supplier.
```

Figure A.1: Data Sheet provided by GEA (Yazbek, 2013)

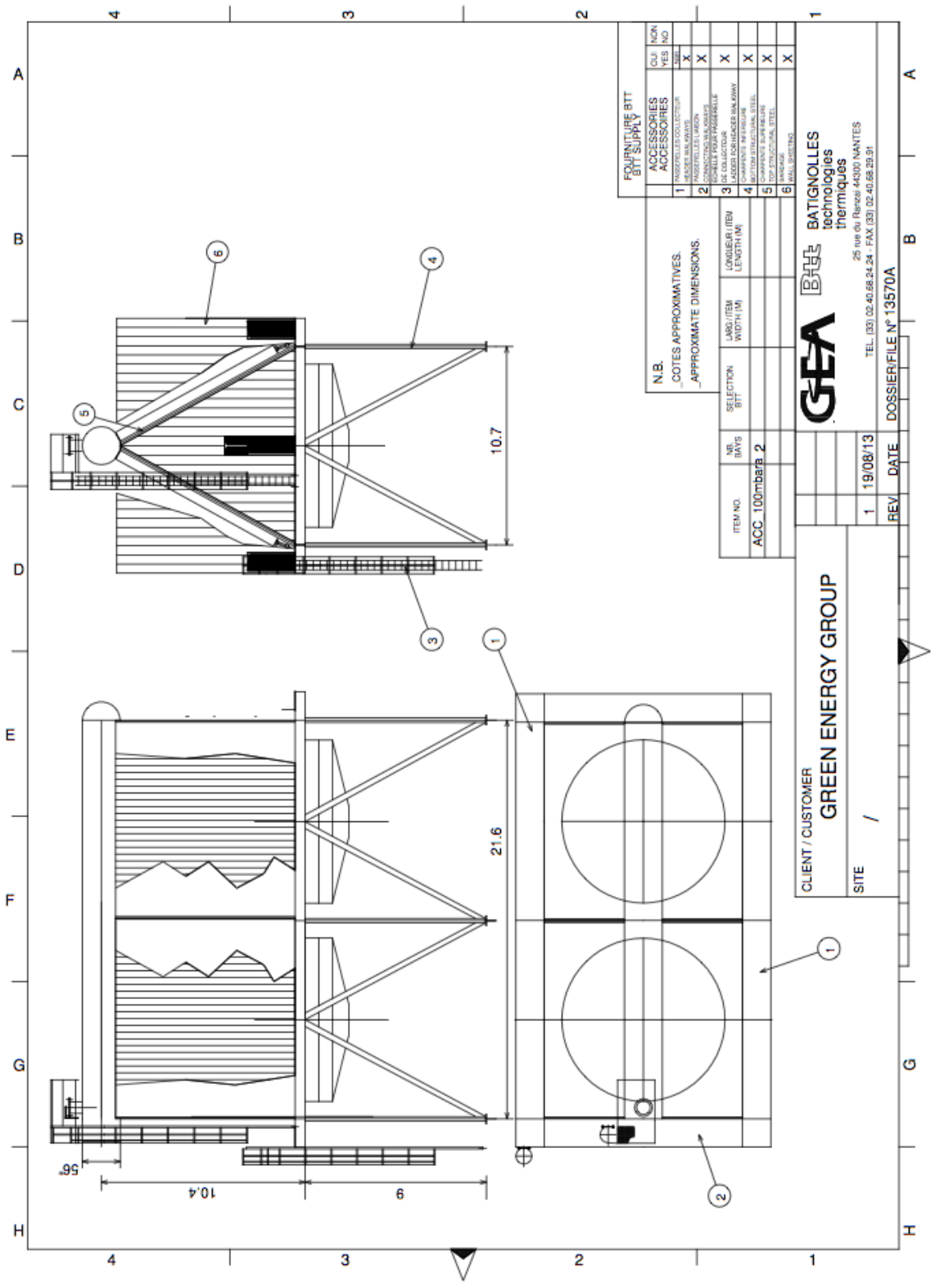

Figure A.2: Schematic provided by GEA (Yazbek, 2013)

B. Fin Efficiency Derivation

Let r represent a coordinate at a distance from the tube center. The variable thickness of the fin can be described as

$$t = \frac{H_f + R - r}{H_f} t_b + \frac{r - R}{H_f} t_t \tag{B.1}$$

where R is the tube outside radius. Therefore, the variable area is represented by

$$A = 2\pi r t = \frac{2\pi r}{H_f}((H_f + R - r)t_b + (r - R)t_t) \tag{B.2}$$

Furthermore, the parameter above and below in a small section dr is found with the following equation

$$P = \frac{4\pi r}{\cos(\theta)} dr \tag{B.3}$$

where

$$\frac{1}{\cos(\theta)} = \frac{\sqrt{\left(\frac{t_b - t_t}{2}\right)^2 + H_f^2}}{H_f} = \sqrt{\left(\frac{t_b - t_t}{2H_f}\right)^2 + 1} \tag{B.4}$$

When $\frac{1}{\cos(\theta)}$ is calculated, it is found to be 1.00002, making $P = 4\pi r dr$.

The energy balance for the fin is now

$$\frac{d}{dr}\left(\frac{2\pi r k_f}{H_f}((H_f + R - r)t_b + (r - R)t_t)\frac{dT}{dr}\right) = 4\pi r h_a (T - T_\infty) \tag{B.5}$$

Dimensionless linear relationships are determined for r_1 and r_2

$$\psi_1 = \frac{r_2 - r}{r_2 - r_1}$$

$$\psi_2 = \frac{r - r_1}{r_2 - r_1}$$

where $T(r) = T_1\psi_1(r) + T_2\psi_2(r)$. The derivatives are

$$\frac{d\psi_1}{dr} = -\frac{1}{r_2 - r_1}$$

$$\frac{d\psi_2}{dr} = \frac{1}{r_2 - r_1}$$

$$\frac{dT}{dr} = \frac{T_2 - T_1}{r_2 - r_1}$$

The weak form of the left side of equation B.5 is

$$\begin{aligned}\int_{r_1}^{r_2} \frac{d\psi}{dr}\frac{2\pi rk}{L}((L+R-r)t_r + (r-R)t_e)\frac{dT}{dr}\,\mathrm{d}r \\ = -\frac{d\psi}{dr}\frac{2\pi rk}{L}\frac{dT}{dr}\int_{r_1}^{r_2}((Lt_r + R(t_r - t_e))r - (t_r - t_e)r^2\,\mathrm{d}r \\ = -\frac{d\psi}{dr}\frac{2\pi rk}{L}\frac{dT}{dr}\left((Lt_r + R(t_r - t_e))\frac{r_2^2 - r_1^2}{2} - (t_r - t_e)\frac{r_2^3 - r_1^3}{3}\right)\end{aligned}$$

for ψ_1 it is

$$\frac{2\pi rk}{L(r_2 - r_1)}\left(\frac{(Lt_r + R(t_r - t_e))(r_2 + r_1)}{2} - \frac{(t_r - t_e)(r_2^2 + r_1r_2 + r_1^2)}{3}\right)(T_2 \;-\; T_1)$$

and for ψ_2 it is

$$\frac{2\pi rk}{L(r_2 - r_1)}\left(\frac{(Lt_r + R(t_r - t_e))(r_2 + r_1)}{2} - \frac{(t_r - t_e)(r_2^2 + r_1r_2 + r_1^2)}{3}\right)(T_1 \;-\; T_2)$$

Similarly, the weak form of the right side of equation B.5 is

$$\begin{aligned}\int_{r_1}^{r_2}\psi_1 4\pi rh(T - T_\infty)\,\mathrm{d}r = \frac{4\pi rh}{r_2 - r_1}\int_{r_1}^{r_2}(r_2 - r)r(T - T_\infty)\,\mathrm{d}r \\ = \frac{4\pi rh}{r_2 - r_1}\int_{r_1}^{r_2}(r_2 - r)r\left(\frac{T_1(r_2 - r) + T_2(r - r_1)}{(r_2 - r_1)} - T_\infty\right)\mathrm{d}r \\ = \frac{\pi h}{3}(r_2 - r_1)(3r_1 + r_2)T_1 + \frac{\pi h}{3}(r_2 - r_1)(r_1 + r_2)T_2 - \frac{2\pi h}{3}(r_2 - r_1)(2r_1 + r_2)T_\infty\end{aligned}$$

and

$$\begin{aligned}\int_{r_1}^{r_2}\psi_2 4\pi rh(T - T_\infty)\,\mathrm{d}r = \frac{4\pi rh}{r_2 - r_1}\int_{r_1}^{r_2}(r - r_1)r(T - T_\infty)\,\mathrm{d}r \\ = \frac{4\pi rh}{r_2 - r_1}\int_{r_1}^{r_2}(r - r_1)r\left(\frac{T_1(r_2 - r) + T_2(r - r_1)}{(r_2 - r_1)} - T_\infty\right)\mathrm{d}r \\ = \frac{\pi h}{3}(r_2 - r_1)(r_1 + r_2)T_1 + \frac{\pi h}{3}(r_2 - r_1)(r_1 + 3r_2)T_2 - \frac{2\pi h}{3}(r_2 - r_1)(r_1 + 2r_2)T_\infty\end{aligned}$$

This can then be combined into a linear equation

$$
\begin{aligned}
-\frac{2\pi rk}{L(r_2-r_1)}\Bigg(&\frac{(Lt_r+R(t_r-t_e))(r_2+r_1)}{2}\\
&-\frac{(t_r-t_e)(r_2^2+r_1r_2+r_1^2)}{3}\Bigg)\begin{bmatrix}1 & -1\\ -1 & 1\end{bmatrix}\begin{bmatrix}T_1\\ T_2\end{bmatrix}\\
&=\frac{\pi h(r_2-r_1)}{3}\begin{bmatrix}(3r_1+r_2) & (r_1+r_2)\\ (r_1+r_2) & (r_1+3r_2)\end{bmatrix}\begin{bmatrix}T_1\\ T_2\end{bmatrix}\\
&\quad-\frac{2\pi h(r_2-r_1)T_\infty}{3}\begin{bmatrix}2r_1+r_2\\ r_1+2r_2\end{bmatrix}
\end{aligned}
$$

Finally, a random condition needs to be assigned to the tip of the fin. This condition is subtracted from the left side of equation B.5

$$2\pi Rt_e h(T-T_\infty)$$

The expression is then solved using the following boundary conditions

$$T_\infty = 0$$

$$T_0 = 1$$

The fin efficiency is then the ratio of actual heat transfer to the fin's maximum heat transfer

$$\eta_{fin} = q_0/q_{max} \tag{B.6}$$

where the maximum fin heat transfer is defined as

$$q_{max} = 2\pi((R_o+H_f)^2-R_o^2)+2\pi(R_o+H_f)t_t)h_a(T_0-T_\infty); \tag{B.7}$$

where R_o is the outside diameter of the tube.

The MATLAB code to solve for fin efficiency is displayed here:

```
function [eta_f, r, T] = etafin(h,n,tb,tt,kfin,Do,Hf)

  R = (Do/2);
  L = Hf;

  Tinf = 0;
  T0 = 1;
  dr = L / n;
  A = sparse(n+1,n+1);
  b = zeros(n+1,1);
  for j = 0:n-1,
      r1 = j*dr + R;
      r2 = (j+1)*dr + R;
      A1 = -2*pi*kfin/(L*(r2-r1))*((L*tb+R*(tb-tt))*(r2+r1)/2 ...
          -(tb-tt)*(r2^2+r2*r1+r1^2)/3)*[1 -1; -1 1];
      A2 = pi*h*(r2-r1)/3*[3*r1+r2 r1+r2; r1+r2 r1+3*r2];
      b1 = -2*pi*h*(r2-r1)*Tinf/3*[2*r1+r2; r1+2*r2];
      A(j+1:j+2,j+1:j+2) = A(j+1:j+2,j+1:j+2) + A1 - A2;
      b(j+1:j+2) = b(j+1:j+2) + b1;
  end
  A(end,end) = A(end,end) - 2*pi*R*tt*h;
  b(end,end) = b(end,end) - 2*pi*R*tt*h*Tinf;
  B = sparse(1,n+1);
  B(1) = 1;
  c = T0;
  x = [A B'; B 0] \ [b; c];
  T = x(1:end-1);
  r = linspace(R,R+L,n+1);
  q0 = x(end);
  qmax = (2*pi*((R+L)^2-R^2)+2*pi*(R+L)*tt)*h*(T0-Tinf);
  eta_f = q0/qmax;
```